
AN ENSEMBLE INFORMATION FILTER: RETRIEVING MARKOV-INFORMATION FROM THE SPDE DISCRETISATION

A PREPRINT

Berent Ånund Strømnes Lunde
Equinor, Bergen, Norway
ber1@equinor.com

January 16, 2025

ABSTRACT

Ensemble-based Data Assimilation faces significant challenges in high-dimensional systems due to spurious correlations and ensemble collapse. These issues arise from estimating dense dependencies with limited ensemble sizes. This paper introduces the Ensemble Information Filter, which encodes Markov properties directly into the statistical model’s precision matrix, leveraging structure from SPDE dynamics to constrain information to propagate locally. EnIF eliminates the need for ad-hoc localisation, improving statistical consistency and scalability. Numerical experiments demonstrate its advantages in filtering, smoothing, and parameter estimation, making EnIF a robust and efficient solution for large-scale data assimilation problems.

Keywords Data assimilation · Ensemble methods · SPDE · Markov · Information filter · Localisation

1 Introduction

Ensemble-based Data Assimilation (EDA) is a cornerstone methodology for integrating observations into dynamical models, particularly in high-dimensional non-linear systems. It sees applications to weather forecasting and meteorology (Houtekamer and Mitchell, 2005), oceanography (Evensen, 1994), and reservoir engineering (Aanonsen et al., 2009). Despite its widespread success, EDA faces critical statistical challenges such as spurious correlations and ensemble collapse. These are typically addressed through localisation techniques (Anderson, 2003; Evensen, 2003; Ott et al., 2004; Hamill et al., 2001; Houtekamer and Mitchell, 2001). The techniques are to some extent in need of manual tuning, and lack theoretical grounding.

This paper makes several contributions toward statistically efficient EDA algorithms that are adaptive, computationally scalable, and easy to use for practitioners.

The first contribution is the framing of statistical EDA problems as well understood supervised learning problems. Marzouk et al. (2016) reformulate EDA as an optimisation problem over the Kullback-Leibler Divergence (KLD) between the prior distribution P and an approximating distribution Q . When taking into account finite ensemble sizes, we unify the understanding of EDA under a statistical learning framework (Hastie et al., 2009). This framing enables us to identify overfitting as a fundamental challenge in traditional methods like the Ensemble Kalman Filter (EnKF) (Evensen, 1994; Burgers et al., 1998) and Ensemble Smoother (ES) (Evensen et al., 2009). Specifically, the optimism of the training loss—due to estimated dependencies in Q being overly confident due to finite ensemble size—correspond to spurious correlations, ensemble collapse, and eventual divergence from P . Addressing these issues requires methods that can regularize Q effectively, balancing model complexity with statistical reliability.

Secondly, Markov properties in P are leveraged to combat overfitting and guide statistical estimation. These properties emerge naturally from the dynamics of the governing models, such as solutions to SPDEs. For smoothing, exact Markov properties are well-established (Lindgren et al., 2011); for filtering, they can be considered an effective parsimonious approximation. Encoding these properties into Q via sparsity constraints not only mitigates spurious correlations, but also enhances scalability by reducing computational complexity (Rue and Held, 2005; Rue et al., 2009; Kristensen et al.,

2016). The resulting locality-driven framework provides a theoretically grounded alternative to ad-hoc localisation approaches.

Thirdly, the paper presents the Ensemble Information Filter (EnIF), a novel approach to EDA that directly encodes Markov properties into the statistical model through sparsity in precision matrices and sparse linear maps. By leveraging theory from triangular measure transport, supervised learning, and SPDEs, EnIF achieves improved statistical consistency without the need for ad-hoc localisation. The author considers it a direct competitor to classical approaches such as the EnKF and ES, offering advantages in convergence, adaptiveness, and scalability.

The paper is laid out as follows: Section 2 introduces EDA and necessary background theory and Section 3 discusses Markov properties for filtering and smoothing under SPDE dynamics. Section 4 describes the proposed EDA algorithm. Section 5 provides experiments focusing on various properties of the methodology, while Section 6 showcase the applicability of the methodology to smoothing, filtering, and parameter estimation. Section 7 provides discussion.

2 Ensemble based data assimilation

Table 1: Nomenclature separated in mathematical, problem setup, statistical, and ensemble-representation blocks

Symbol	Description
x	scalar
\mathbf{x}	vector (bold font)
\mathbf{X}	matrix (capitalised bold font)
$\text{tr}(\cdot)$	the trace operator $\text{tr}(\mathbf{X}) = \sum_j \mathbf{X}_{j,j}$
Δ, ∇, ∇^2	finite differences, gradient, and Hessian operators
$\text{div} \nabla$	the Laplacian operator as divergence of the gradient field
$\mathcal{G} = (\mathcal{V}, \mathcal{E})$	graph with vertices \mathcal{V} and edges \mathcal{E}
$\text{ne}(i)$	set of neighbours j having an edge to vertex i in \mathcal{G}
<hr style="border-top: 1px dashed black;"/>	
\mathbf{x}	spatial coordinates
$u_t(\mathbf{x})$	the state, a random field indexed by both time t and space \mathbf{x}
\mathbf{u}_t	state vector at t of state elements over discretised space
$\mathbf{u} = [\mathbf{u}_1, \dots, \mathbf{u}_T]^\top$	state vector at discretised indexed times $1 \leq t \leq T$
\mathbf{y}_t	response of map $\mathbf{y}_t = \mathbf{h}_t(\mathbf{u}_t)$ on state, often simply $\mathbf{h}(\mathbf{u}_t) = \mathbf{H}\mathbf{u}_t$
\mathbf{d}_t	noisy observation of response, $\mathbf{d}_t = \mathbf{y}_t + \boldsymbol{\epsilon}_t$, $\boldsymbol{\epsilon}_t \sim N(\mathbf{0}, \boldsymbol{\Sigma}_{\boldsymbol{\epsilon}_t})$ at t
$\mathbf{u}_{t s}$	state random variable \mathbf{u}_t conditioned on observations \mathbf{d} up until time s
$\mathbf{u} \mathbf{d}_T, \mathbf{u} \mathbf{d}_t, \boldsymbol{\theta} \mathbf{d}_t$	smoothing, filtering, and parameter estimation problems
<hr style="border-top: 1px dashed black;"/>	
$p(\mathbf{u})$	probability density function of a random vector \mathbf{u}
$\mathbf{u} \perp \mathbf{v}$	independence of \mathbf{u} and \mathbf{v} , $p(\mathbf{x}, \mathbf{y}) = p(\mathbf{x})p(\mathbf{y})$ factorises
$\mathbb{E}[\mathbf{u}]$	expectation operator $\mathbb{E}[\mathbf{u}] = \int p(\mathbf{u}) d\mathbf{u}$
$\boldsymbol{\mu}, \boldsymbol{\Sigma}$	mean $\boldsymbol{\mu} = \mathbb{E}[\mathbf{u}]$ and covariance $\boldsymbol{\Sigma} = \mathbb{E}[(\mathbf{u} - \boldsymbol{\mu})(\mathbf{u} - \boldsymbol{\mu})^\top]$
$\boldsymbol{\Sigma}^*$	sample-covariance estimate
$\boldsymbol{\eta}, \boldsymbol{\Lambda}$	canonical parametrisation $\boldsymbol{\eta} = \boldsymbol{\Lambda}\boldsymbol{\mu}$ and $\boldsymbol{\Lambda} = \boldsymbol{\Sigma}^{-1}$
$\text{Prec}(\cdot)$	precision matrix operator $\text{Prec}(\mathbf{u}) = \boldsymbol{\Lambda}_\mathbf{u}$
$D_{\text{KL}}(P Q)$	Kullback-Leibler divergence of (truth) $p_P(\mathbf{u})$ from (model) $p_Q(\mathbf{u})$
<hr style="border-top: 1px dashed black;"/>	
$\mathbf{u}^{(i)}$	realisation sampled from $\mathbf{u}^{(i)} \sim p(\mathbf{u})$
$\mathbf{y}^{(i)}, \mathbf{d}^{(i)}$	response, $\mathbf{y}^{(i)} = \mathbf{h}(\mathbf{u}^{(i)})$, and noisy response, $\mathbf{d}^{(i)} = \mathbf{y}^{(i)} + \boldsymbol{\epsilon}^{(i)}$, realisations
$\mathbf{u}_{i t-1}^{(i)}, \mathbf{u}_{i t}^{(i)}, \mathbf{u}_{i T}^{(i)}$	prior, posterior filter and posterior smoothing realisation
$1 \leq i \leq n$	realisation index (typically in parenthesised superscript $\mathbf{u}_i^{(i)}$)
$1 \leq (s, t) \leq T$	time indexation, typically in subscripts
$1 \leq k \leq p_x$	spatial position index of \mathbf{x} in a discretised field
$1 \leq j \leq p$	parameter index (dimensions of \mathbf{u} or \mathbf{u}_t), enumerates combinations of t and k
$\mathcal{G}_\mathbf{u}, \mathcal{G}_\mathbf{x}$	graphs defining relations between parameters and points in space

This section introduces the necessary background. Detailed nomenclature is provided in Table 1. Familiarity with the following three fields, with suggested references, are helpful:

- Gaussian Markov random fields (GMRF) (Rue and Held, 2005) and their relation to stochastic partial differential equations (SPDE) (Lindgren et al., 2011, 2022).

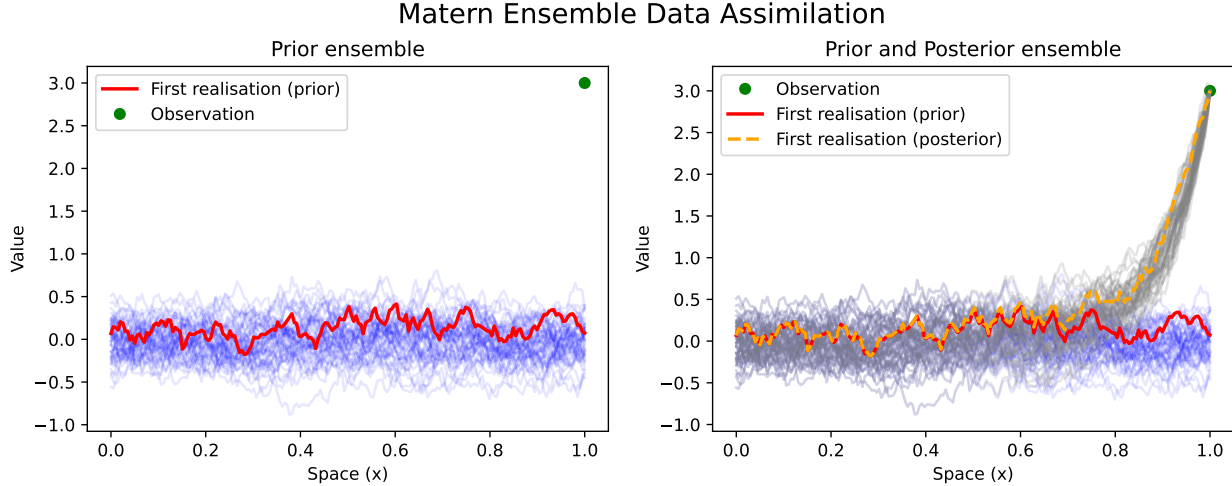


Figure 1: Left: 50 realisations of 1-d Matérn ($\kappa = 0.1$) Gaussian process as in Example 1 sampled on $x \in [0, 1]$, unconditioned on an observation of the endpoint (green dot) at $x = 1.0$. Right: Conditioned realisations overlayed the unconditional ones from the left plot. The update is a special case of the EnKF and is expressed in Example 1. Red line showcases the first Matérn realisation (left) and how this realisation is updated (orange, right).

- Classical ensemble based data assimilation (Evensen et al., 2009) and Bayesian consistent assimilation through methods of triangular measure transport (Marzouk et al., 2016; Baptista et al., 2020; Ramgraber et al., 2023a).
- Supervised learning (Hastie et al., 2009) and the relation of statistical complexity to overfitting (Akaike, 1974; Claeskens and Hjort, 2008).

2.1 Dynamical model conditioned on observations

Data assimilation (DA) consists of observations or data and a (dynamical forward) model. As the forward model, we take a solution g of the time-homogeneous stochastic process, $u_t(\mathbf{x})$ named the *state*, defined via the SPDE

$$\mathcal{L}u_t(\mathbf{x}) = \mathcal{A}u_t(\mathbf{x}) + \sigma(u_t(\mathbf{x}))\mathcal{W}_t(\mathbf{x}). \quad (1)$$

It consists of spatial and temporal model operators \mathcal{A} and \mathcal{L} , and a (stochastic) diffusion term σ as $\mathcal{W}_t(\mathbf{x})$ is a white noise process. This is a similar model as in the classical DA literature (Evensen et al., 2009, Chap. 4.3.2, p.39). But, we are explicit that both \mathcal{A} and \mathcal{L} are local operators, and only work on a neighbourhood of $u_t(\mathbf{x})$ in time and space (e.g. differential operators or functions on $u_t(\mathbf{x})$ directly). The operator \mathcal{L} relates to derivatives in time. We assume $\mathcal{W}_t(\mathbf{x})$ to be the differential of a spatio-temporal Wiener process, and take the integral to be the Ito integral, see e.g. Øksendal (2003). All three operators may depend on a set of parameters θ that may be taken as deterministic or stochastic. Unless otherwise stated, assume θ to be deterministic and their inclusion in g implicit.

The second key component is (uncertain or noisily observed) data, $\mathbf{d}_t \sim p_{\mathbf{d}}$. The observations are assumed related to the state through a (possibly stochastic) map \mathbf{h} . Necessarily, the observations also yield information regarding \mathbf{u} . The goal of DA is to retrieve information on the posterior of the state $\mathbf{u}|\mathbf{d}$.

An ensemble based data assimilation (EDA) approach simulates realisations $\mathbf{u}_{t|t-1}^{(i)} = g\left(\mathbf{u}_{t-1|t-1}^{(i)}\right)$ through Monte Carlo sampling of the initial state $\mathbf{u}_{t-1|t-1}^{(i)}$ and typically numerical integration of Equation (1). The goal of EDA is then to update each realisation, mapping $\mathbf{u}_{t|t-1}^{(i)}$ to $\mathbf{u}_{t|t}^{(i)}$, so that $\mathbf{u}_{t|t}^{(i)} \sim p(\mathbf{u}_t|\mathbf{d}_t)$.

Example 1 (Conditioned Matérn-GRF). *The Matérn SPDE with $\nu = \frac{1}{2}$ and taken in one dimension is*

$$\left(\kappa^2 - \frac{d^2}{dx^2}\right)^{1/2} u(x) = \mathcal{W}(x). \quad (2)$$

The solution is a stationary mean-zero Gaussian process with covariance function $\text{Cov}(u_x, u_{x+h}) = \frac{\kappa}{2} e^{-\kappa^{-1}|h|}$. It is Markov and has a mean-reverting property. Assume we observe $d_p = u(p) + \epsilon$ a direct but noisy observation of $u(p)$

with $\epsilon \sim \mathcal{N}(0, \sigma_\epsilon^2)$. Simulate $i = 1, \dots, n$ realisations of $u_{x|x_0}$ at $x = 1, 2, \dots, p$, and add simulated noise $\epsilon^{(i)}$ to each $u_{(p)}^{(i)}$ obtaining simulations of d_p . Then update each realisation element (indexed by x) as

$$u_{x|p}^{(i)} = u_{x|0}^{(i)} - \frac{\text{Cov}(u_x, u_p)}{\text{Cov}(u_p, u_p) + \sigma_\epsilon^2} \left(d_p^{(i)} - d_p \right) = u_{x|0}^{(i)} - \frac{\kappa e^{-\kappa^{-1}|p-x|}}{\kappa + 2\sigma_\epsilon^2} \left(d_p^{(i)} - d_p \right) \quad (3)$$

yielding updated realisations $\mathbf{u}^{(i)} = [u_{1|p}^{(i)}, \dots, u_{p|p}^{(i)}]^\top \sim p(\mathbf{u}|\mathbf{d}_p)$.

Notice how in Example 1 we simulated both \mathbf{u} and \mathbf{d} , and employed the joint Gaussian P on (\mathbf{u}, \mathbf{d}) . In most situations the true distributions P is unknown. This is the reason for the ensemble approach, as realisations will be correctly sampled from P . An approximation Q to P may then be estimated from the ensemble, and employed for the conditioning upon \mathbf{d} .

2.2 Consistent ensemble based data assimilation

Arguably, the most promising general purpose way to estimate Q for $\boldsymbol{\nu} = [\mathbf{u}, \mathbf{d}]^\top$ and update an ensemble is through Triangular Measure Transport (Marzouk et al., 2016; Baptista et al., 2020). Measure transport relies on the change of variable formulae

$$p_{\boldsymbol{\nu}}(\boldsymbol{\nu}) = p_{\mathbf{z}}(\mathbf{S}(\boldsymbol{\nu})) \det \nabla \mathbf{S}(\boldsymbol{\nu}) \quad (4)$$

to define the density $p_{\boldsymbol{\nu}}$ through a reference density $p_{\mathbf{z}}$ and a monotone map \mathbf{S} . Triangular measure transport is obtained through structuring the map \mathbf{S} as the *Knothe-Rosenblatt* (KR) *rearrangement* (Rosenblatt, 1952)

$$\mathbf{S}(\boldsymbol{\nu}) = \begin{bmatrix} S_1(\nu_1) \\ S_2(\nu_1, \nu_2) \\ \vdots \\ S_p(\nu_1, \dots, \nu_p) \end{bmatrix} = \begin{bmatrix} z_1 \\ z_2 \\ \vdots \\ z_p \end{bmatrix} = \mathbf{z}. \quad (5)$$

This choice essentially limits the space of possible transport maps to those that are monotone and bijective (Marzouk et al., 2016). Note that the KR map, along with letting the reference $p_{\mathbf{z}}$ be the standard Gaussian, is the exact choice of recent research towards consistent data assimilation through triangular transport (Spantini et al., 2019; Baptista et al., 2020, 2021; Ramgraber et al., 2023a).

A Bayesian update of the prior ensemble can be done through the inverse KR map. Characterise \mathbf{d} through the change of variable formulae with a standard Gaussian reference and the KR map $\mathbf{S}_{\mathbf{d}}$. The joint KR map becomes

$$\mathbf{S}(\mathbf{d}, \mathbf{u}) = \begin{bmatrix} S_1(d_1) \\ \vdots \\ S_m(d_1, \dots, d_m) \\ S_{m+1}(d_1, \dots, d_m, u_1) \\ \vdots \\ S_{m+p}(d_1, \dots, d_m, u_1, \dots, u_p) \end{bmatrix} = \begin{bmatrix} S_{\mathbf{d}}(\mathbf{d}) \\ S_{\mathbf{u}}(\mathbf{d}, \mathbf{u}) \end{bmatrix} = \begin{bmatrix} z_1 \\ \vdots \\ z_{m+p} \end{bmatrix} = \mathbf{z}. \quad (6)$$

Using the properties of the inverse, we may sample from the conditional $p(\mathbf{u}|\mathbf{d})$ through inversion of $\mathbf{u} \mapsto S_{\mathbf{u}}(\mathbf{d}, \mathbf{u})$ working with the lower block of the joint KR map. We might either

1. Sample $\mathbf{z} \sim \mathcal{N}(0, \mathbf{I}_p)$ and evaluate $\mathbf{u} = S_{\mathbf{u}}^{-1}(\mathbf{d}, \mathbf{z}) \sim p(\mathbf{u}|\mathbf{d})$, which works if \mathbf{S} is exact.
2. First sample $\tilde{\mathbf{z}}^{(i)}$ using a training sample / ensemble realisation $(\mathbf{u}_{t|t-1}^{(i)}, \mathbf{d}_t^{(i)})$ evaluating $\tilde{\mathbf{z}}^{(i)} = S_{\mathbf{u}}(\mathbf{u}_{t|t-1}^{(i)}, \mathbf{d}_t^{(i)})$. Then, sample from $p(\mathbf{u}|\mathbf{d}_t)$ evaluating $\mathbf{u}_{t|t}^{(i)} = S_{\mathbf{u}}^{-1}(\mathbf{d}_t, \tilde{\mathbf{z}}^{(i)})$. We here use subscript conditional notation to differentiate prior and posterior updated realisation.

The second approach can be shown to work better because approximations in a learned map $\hat{\mathbf{S}}$ can be shown to cancel when writing the second step as a composite map

$$\mathbf{u}_{t|t}^{(i)} = S_{\mathbf{u}}^{-1}(\mathbf{d}_t, \cdot) \circ S_{\mathbf{u}}(\mathbf{u}_{t|t-1}^{(i)}, \mathbf{d}_t^{(i)}). \quad (7)$$

The KR choice allows learning Q through marginal regressions S_j 's from separating the joint relative Kullback-Leibler Divergence (KLD) (see Ramgraber et al. (2023a))

$$D_{\text{KL}}(P||Q) = E_P [\log p_P(u)] - E_P [\log p_Q(u)] \quad (8)$$

leading to minimisation of the following objective

$$\mathcal{J}_j(S_j) = E_P \left[\frac{1}{2} S_j(\nu_1, \dots, \nu_j)^2 - \log \frac{\partial S_j(\nu_1, \dots, \nu_j)}{\partial \nu_j} \right] \quad (9)$$

for each row j in \mathbf{S} . Here the choice of a standard Gaussian reference has been used. The following example is from Ramgraber et al. (2023a, Appendix B)

Example 2 (Affine Triangular Measure Transport). *Let \mathbf{S} be affine and choose the reference $p_{\mathbf{z}}$ as standard Gaussian. Then*

$$\mathbf{S}(\boldsymbol{\nu}) = \mathbf{C}\boldsymbol{\nu} = \begin{bmatrix} c_{1,1} & & & \\ c_{2,1} & c_{2,2} & & \\ \vdots & \vdots & \ddots & \\ c_{p,1} & c_{p,2} & \dots & c_{p,p} \end{bmatrix} \begin{bmatrix} \nu_1 \\ \nu_2 \\ \vdots \\ \nu_p \end{bmatrix} \quad (10)$$

yields Q as multivariate Gaussian with precision $\boldsymbol{\Lambda} = \mathbf{C}^\top \mathbf{C} = \boldsymbol{\Sigma}^{-1}$. Furthermore, the composite map (7) retrieves Gaussian conditioning

$$\mathbf{u}_{t|t}^{(i)} = \mathbf{u}_{t|t-1}^{(i)} - \boldsymbol{\Sigma}_{\mathbf{u},\mathbf{d}} \boldsymbol{\Sigma}_{\mathbf{d}}^{-1} (\mathbf{d}_{t|t-1}^{(i)} - \mathbf{d}_t). \quad (11)$$

Note how the update in Example 1 is a special case.

If Equation (9) could be solved, then it is likely that $Q = P$ can be found. If P is non-Gaussian but \mathbf{S} is constrained to be linear like \mathbf{C} in Example 2, then the population estimate of covariance will be found by optimising (9) and subsequently used in the update (11). In practice, the idealised objective (9) is exchanged with its sample estimator, using the ensemble. This simple swap, if done naively and at large dimension $p + m$ of $\boldsymbol{\nu}$ at finite ensemble sizes n , has severe consequences like spurious correlations and ensemble collapse.

2.3 Supervised learning of the statistical model Q

Because P is unknown, and we use the KLD from Equation (8), we replace Equation (9) with its sample estimator using the ensemble. Let $\boldsymbol{\theta}$ parameterise Q . Then, population quantities

$$\boldsymbol{\theta}_0 = \arg \min_{\boldsymbol{\theta}} -E_P [\log p_Q(\mathbf{u}; \boldsymbol{\theta})] \quad (12)$$

are replaced with the likelihood estimator

$$\hat{\boldsymbol{\theta}} = \arg \min_{\boldsymbol{\theta}} -\frac{1}{n} \sum_{i=1}^n \log p_Q(\mathbf{u}^{(i)}; \boldsymbol{\theta}). \quad (13)$$

Under regularity conditions, $\hat{\boldsymbol{\theta}}$ is asymptotically unbiased and is the minimum variance estimator (AUMVE) (Van der Vaart, 2000). At finite sample/ensemble sizes, $\hat{\boldsymbol{\theta}}$ has non-zero variance. Thus, even if the model (1) dictates local behaviour and zero correlations for distant points, the estimated dependence in sample covariance (typically taken as $\boldsymbol{\theta}$ in EDA) will still be non-zero with probability one. This is known as spurious correlations in the literature.

Example 3 (Ensemble Smoother on Matérn). *Let \mathbf{C} in Example 2 be learned dense from Matérn data in Example 1, optimising the empirical version (13) of (9). For $p \geq n$ and otherwise under suitable conditions, we obtain a covariance estimate close to the sample covariance estimate. Inserting the sample covariance into (11), we obtain an Ensemble Kalman Smoother (Evensen et al., 2009). Figure 2 (left) showcase an update of the unconditioned Matérn realisations of Example 1 using the Ensemble Smoother. The right plot showcase the ensemble sample-correlations used for the update, along with additionally sampled sample-correlations and confidence bands that are functions of ensemble size.*

Example 3 with Figure 2 illustrate how the estimated correlations far from the observation are non-zero and induce a noisy update. The unfortunate effect fortunately goes to zero at an infinite ensemble size, as the variance of the statistical estimate is $\mathcal{O}(n^{-1})$ (middle plot).

A second unfortunate effect occurs after propagating a Bayesian update through the spurious correlations: Doing this leads to an unwarranted decrease in uncertainty. It is a function of unwarranted (spurious) estimated strength of the dependence, and the number of times one propagates a Bayesian update, i.e. the number of observations one conditions on. If (nearly) all uncertainty in one or multiple variables is lost to spurious updates, all ensemble members will share (near-identical) values in those variables. This loss of variation is known as ensemble collapse. This effect, even with only one observation, is clear when comparing the width of the posterior ensembles of Examples 1 and 2.

In the EDA literature, these statistical issues have received much attention. Two classes of solutions worth mentioning are:

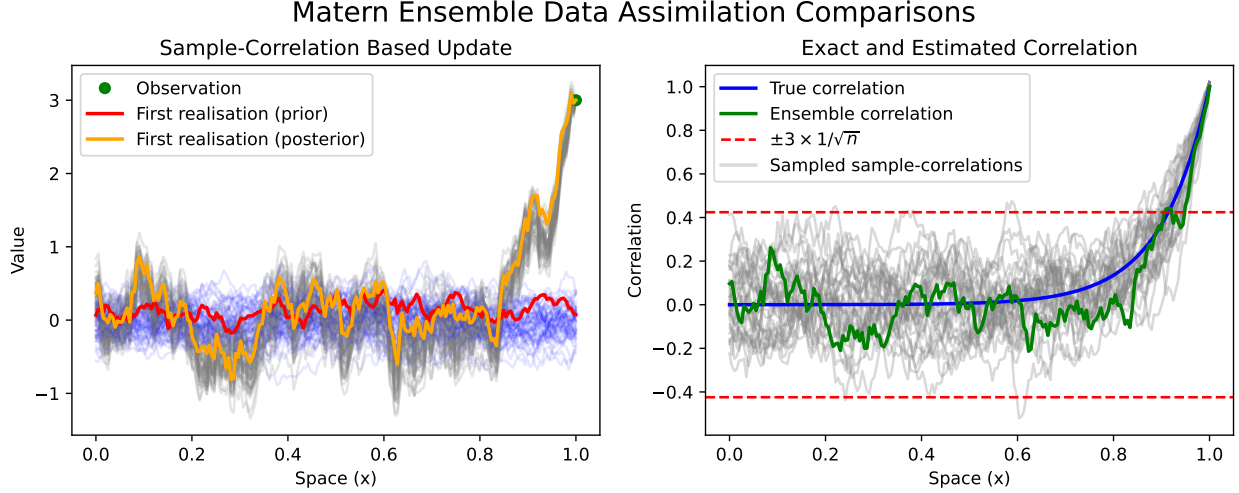


Figure 2: Left: Conditioned realisations as in Figure 1 right, but exchanging true covariance with sample covariance using the 50 unconditioned Matérn realisations. Right: 30 different sample correlations with the endpoint $x = 1.0$ based on $n = 50$ realisations, along with the true population correlation. The green line is the exact sample-correlations used for the update in the left plot.

- **Distance-based localisation** (Houtekamer and Mitchell, 2001; Anderson, 2003; Hunt et al., 2007) reduces the update to zero based on distance. A kernel function, such as the Gaussian kernel $\exp -c\delta^2$, is used, with c controlling the radius of influence.
- **Adaptive localisation** involves regression $h^{-1} : \mathbf{d} \mapsto \mathbf{u}$ (with \mathbf{K} as the asymptotic solution) and model selection. If the sample correlation between $(\mathbf{u}_j, \mathbf{d}_k)$ is smaller than a threshold (e.g. $3/\sqrt{n}$), the effect in \mathbf{K} is set to zero. Otherwise, it is computed normally.

The KLD perspective (8) provides more insight into EDA's statistical issues than just the variance of the sample covariance. When we exchange (12) with (13), we implicitly integrate over the empirical distribution function P^* :

$$-\frac{1}{n} \sum_{i=1}^n \log p_Q(\mathbf{u}^{(i)}; \boldsymbol{\theta}) = -E_{P^*} [\log p_Q(\mathbf{u}; \boldsymbol{\theta})]. \quad (14)$$

Since $Q(\hat{\boldsymbol{\theta}})$ is closer to P^* than P in the KLD sense, there is an expected bias $B(\hat{\boldsymbol{\theta}}) > 0$ when subtracted from the expectation under P (Konishi and Kitagawa, 1996). Furthermore, $B(\hat{\boldsymbol{\theta}})$ increases with the complexity of $\boldsymbol{\theta}$. If $\boldsymbol{\theta}$ has unnecessary degrees of freedom, it increases $B(\hat{\boldsymbol{\theta}})$ and the unwanted divergence from Q to P .

Under regularity conditions, the bias $B(\hat{\boldsymbol{\theta}})$ may be approximated as:

$$B(\hat{\boldsymbol{\theta}}) \approx \text{tr} \left(\mathcal{H}(\boldsymbol{\theta}_0) \text{Cov}(\hat{\boldsymbol{\theta}}) \right), \text{ where } \mathcal{H}(\boldsymbol{\theta}_0) = -E_P \left[\nabla_{\boldsymbol{\theta}_0}^2 \log p_Q(\mathbf{u}; \boldsymbol{\theta}_0) \right]. \quad (15)$$

Using the Sandwich estimator (Huber et al., 1967) and empirical Hessian, we arrive at the TIC (Takeuchi, 1976). The expression for $B(\hat{\boldsymbol{\theta}})$ can also be related to effective degrees of freedom in $Q(\boldsymbol{\theta})$ (Hastie et al., 2009). If $P = Q(\boldsymbol{\theta}_0)$, then $B(\hat{\boldsymbol{\theta}}) = \text{len}(\boldsymbol{\theta})$, recovering the celebrated AIC (Akaike, 1974).

This poses a problem for classical EDA: using the sample covariance, $\text{len}(\boldsymbol{\theta})$ is quadratic in p , while the data-ensemble grows only linearly with increased resolution. Figure 3 shows how the numerical scheme can improve with resolution while EDA using the sample covariance (EnKF/ES) only improves initially before statistical noise dominates through an increase in $B(\hat{\boldsymbol{\theta}})$.

Solutions to (1) are provided through numerical methods (e.g., finite element (FEM) or finite difference methods (FDM)) that improve at increased resolution; Δx and Δt approaching zero. Fitting a high-resolution statistical model $Q(\hat{\boldsymbol{\theta}})$ close to P or $Q(\boldsymbol{\theta}_0)$ for conditioning on \mathbf{d} is non-trivial. If done naively, like with the sample covariance, the statistical model will diverge from P .

Fortunately, the KLD perspective provides insight into tools to limit divergence, as seen in Equation (15) for $B(\hat{\theta})$. Our goal is the minimisation of the bias-corrected negative log-likelihood:

$$-E_P [\log p_Q(\mathbf{u}; \boldsymbol{\theta})] \approx -E_{P^*} [\log p_Q(\mathbf{u}; \boldsymbol{\theta})] + B(\hat{\theta}). \quad (16)$$

To this end, we may:

- **Use structure** to limit the size of $\boldsymbol{\theta}$ by constraining the search to a suitable subspace of the full parameter space.
- **Use regularisation** to trade variance in $\boldsymbol{\theta}$ for some bias. This makes the empirical negative log-likelihood larger but benefits from a smaller B , ultimately reducing the expression. Hastie et al. (2009) discuss such techniques extensively.

It is important to encode both structure and regularisation before statistical fitting. This ensures that estimates $\hat{\theta}$ have optimal properties and adapt to the simulated data in the ensemble.

Regularisation alone cannot solve the aforementioned resolution problem. At higher resolutions, statistical noise dominates (unless structure is informed upon), and optimal regularisation will zero out interactions (e.g., $\mathbf{K} = \mathbf{0}$), retaining the prior. Thus, structure is needed. Fortunately, the numerical solution of the SPDE model (1) provides structure in P .

3 Markov structure from local operators

A key difference between ordinary supervised learning and EDA is the presence of the model in Equation (1), which encodes domain knowledge. When such a model is unavailable, a locality approach is often used in an ad-hoc manner. In spatio-temporal models, Markov properties are frequently employed due to their theoretical and computational benefits.

Markov properties naturally arise in both analytical and numerical solutions to the model (1). They reduce the degrees of freedom, capture essential local spatial effects, and enable efficient computation. Unlike distance-based localisation, Markov properties may encode local dependence structures directly into the parameters, given an appropriate parametrisation.

From Rue and Held (2005), if $\mathcal{G} = (\mathcal{V}, \mathcal{E})$ is a graph with vertices \mathcal{V} and edges \mathcal{E} , a random vector $\mathbf{u} \in \mathbb{R}^d$ is a Gaussian Markov Random Field (GMRF) with respect to $\mathcal{G} = (1, \dots, d, \mathcal{E})$, mean $\boldsymbol{\mu}$, and SPD precision matrix $\boldsymbol{\Lambda} = \boldsymbol{\Sigma}^{-1}$, if:

$$p(\mathbf{u}) = (2\pi)^{-\frac{d}{2}} \sqrt{|\boldsymbol{\Lambda}|} \exp\left(-\frac{1}{2}(\mathbf{u} - \boldsymbol{\mu})^\top \boldsymbol{\Lambda}(\mathbf{u} - \boldsymbol{\mu})\right) \quad (17)$$

and

$$\Lambda_{i,j} \neq 0 \Leftrightarrow (i,j) \in \mathcal{E} \quad \forall i \neq j. \quad (18)$$

Thus, the space of precision matrices is limited to the subspace of SPD matrices with exact zeroes corresponding to no edge in \mathcal{G} . The length of the statistical parameter vector $\boldsymbol{\theta}$ is therefore $m + l$, the number of vertices m and edges l in \mathcal{G} . The sample covariance corresponds to a fully connected \mathcal{G} with $l = O(m^2)$, which is problematic. Local connections in \mathcal{E} resolve this issue.

In terms of continuous solutions to (1), Rozanov (1977) finds that for linear SPDEs of the form

$$\mathcal{L}u(\mathbf{x}) = \mathcal{W}(\cdot), \quad (19)$$

the solutions are Gaussian random fields. When \mathcal{L} only involves local operators, they also have the Markov property. In particular, note that the precision operator, \mathcal{Q} , is found directly as $\mathcal{Q} = \mathcal{L}^* \mathcal{L}$, where \mathcal{L}^* is the adjoint of \mathcal{L} . Thus the Markov property stems from the locality of the operators, as \mathcal{Q} will only involve this through \mathcal{L} .

Example 4 (Markov solutions to the Matérn SPDE). *The general Matérn SPDE is given by*

$$(\kappa^2 - \text{div } \nabla)^{\frac{\alpha}{2}} \mathbf{u}(\mathbf{x}) = \mathcal{W}(\mathbf{x}), \quad (20)$$

which is a fractional linear SPDE. The solution is Gaussian, and in the case of integer powers of α , the precision operator $(\kappa^2 - \text{div } \nabla)^\alpha$ can be expanded into a sum of integer powers of the negated Laplacian (Lindgren et al., 2022).

Thus \mathcal{L} is linear and involves only ordinary local operators and is therefore also Markov. In the non-integer case, the negative fractional Laplacian is given by

$$(-\operatorname{div} \nabla)^{\frac{\alpha}{2}} \mathbf{u}(\mathbf{x}) = C_{\alpha,d} \int_{\mathbb{R}^d} \frac{\mathbf{u}(\mathbf{x}) - \mathbf{u}(\mathbf{y})}{|\mathbf{x} - \mathbf{y}|^{d+\alpha}} d\mathbf{y}, \quad (21)$$

and is a global/non-local operator. The solution is still Gaussian, but not Markov. Due to the "kernel" $\frac{1}{|\mathbf{x}-\mathbf{y}|^{d+\alpha}}$, there is, however, still an importance to locality, as the influence of distant points \mathbf{y} decreases with distance.

In EDA the target distribution P is not defined through the exact solution of (1), but rather the discretised numerical simulation. But here, too, Markov properties arise. Specifically, we will see that

- For EDA smoothing problems, a theoretical argument can (often) be made for exact Markov properties.
- For EDA filtering problems, a theoretical argument can be made for a Markov approximation, if the argument for the smoothing problem is valid.
- For EDA parameter estimation, a separate argument can be made for Markov properties and sparsity.

3.1 Numerical solutions and Markov properties for smoothing

If a local and therefore sparse numerical (approximate) solution is feasible to P , then so is the Markov assumption. We will here provide links for the finite difference method (FDM) and finite element method (FEM) case. The FDM is relatively straightforward, while the FEM is via the celebrated SPDE approach of Lindgren et al. (2011).

If P is defined via a FDM solution to (1) on a discretised (spatio-temporal) grid, the sparsity of the precision is direct. As the operators are assumed local, a FDM approximation for $u_{t_k}(\mathbf{x}_j)$ (where j and k indexes the grid) will involve only the value of u at the neighbours of j and k . For instance, $\tilde{\mathbf{L}}$ as a finite dimensional approximation to \mathcal{L} in (19) will be band-sparse, which will carry over to sparsity in $\mathbf{\Lambda}_u = \tilde{\mathbf{Q}} = \tilde{\mathbf{L}}^\top \tilde{\mathbf{L}}$. The sparsity of $\mathbf{\Lambda}$ implies conditional independence and Markov properties.

FEM are applicable for a larger class of models (1). The link to Markov properties are due to Lindgren et al. (2011) through some explicit choices. To illustrate the approach, we make use of a simple version of (1)

$$\frac{d}{dt} u_t(\mathbf{x}) - \mathcal{A}u_t(\mathbf{x}) = \sigma \mathcal{W}. \quad (22)$$

The SPDE approach seeks a stochastic weak solution, so that for a suitable set of test-functions $v(\mathbf{x})$ we seek equality in distribution for

$$\int_{\Omega} v(\mathbf{x}) \left(\frac{d}{dt} u_t(\mathbf{x}) - \mathcal{A}u_t(\mathbf{x}) \right) d\mathbf{x} \stackrel{d}{=} \sigma \int_{\Omega} v(\mathbf{x}) \mathcal{W}(t, \mathbf{x}) d\mathbf{x}, \quad (23)$$

where Ω represents the spatial domain. We note that boundary conditions are omitted, as they impose constraints localised to the boundary of Ω . Therefore they do not fundamentally affect the Markov properties of the solution within the domains interior.

The FEM solution represents $u_t(\mathbf{x})$ via basis functions ϕ and values of u at the vertices of a triangular mesh (discretising the field) \mathbf{u} so that

$$u_t(\mathbf{x}) \approx \sum_{k=1}^{p_{\infty}} \mathbf{u}_k(t) \phi_k(\mathbf{x}), \quad (24)$$

where internal values are triangularized. The SPDE approach selects ϕ to be piecewise linear functions so that $\phi_k = 1$ at vertex k , but zero at all other vertices. This choice along with e.g. the Galerkin method (v are chosen from the same family as the basis functions, specifically we select $v = \phi_k$) leads to the matrices

$$\mathbf{M}_{ij} = \int_{\Omega} \phi_j(\mathbf{x}) \phi_i(\mathbf{x}) d\mathbf{x}, \quad (25)$$

$$\mathbf{A}_{ij} = \int_{\Omega} \phi_j(\mathbf{x}) \mathcal{A} \phi_i(\mathbf{x}) d\mathbf{x}. \quad (26)$$

The matrix \mathbf{M} is band-sparse due the choice of basis ϕ , while the same applies to \mathbf{A} if in addition \mathcal{A} is a local operator. Taking the r.h.s. of Equation (23) as the Ito integral, the solution is mean-zero Gaussian. The matrix \mathbf{M} also appears, as

$$\operatorname{Cov} \left(\sigma \int_{\Omega} \phi_i(\mathbf{x}) \mathcal{W}(\mathbf{x}) d\mathbf{x}, \sigma \int_{\Omega} \phi_j(\mathbf{x}) \mathcal{W}(\mathbf{x}) d\mathbf{x} \right) = \sigma^2 \int_{\Omega} \phi_i(\mathbf{x}) \phi_j(\mathbf{x}) d\mathbf{x} = \sigma^2 \mathbf{M}_{ij}. \quad (27)$$

All spatial white-noise is integrated out, so we are left only with white-in-time noise. Thus, the weak solution obtains the sparse SDE system

$$M \frac{d\mathbf{u}}{dt} - \mathbf{A}\mathbf{u} = \sigma M^{\frac{1}{2}} d\mathbf{Z}, \quad (28)$$

where $\mathbf{Z} \sim \mathcal{N}(0, \mathbf{I})$ is due to independent white noise in time. A simple Euler-Maruyama method (Kloeden and Platen, 1992) then achieves

$$M \frac{\mathbf{u}_{t+1} - \mathbf{u}_t}{\Delta t} - \mathbf{A}\mathbf{u}_t = \sigma \Delta t M^{\frac{1}{2}} \mathbf{Z}. \quad (29)$$

Solving, we then see an auto-regressive relationship in time

$$\mathbf{u}_{t+1} = \mathbf{B}\mathbf{u}_t + \mathbf{w}_t, \quad (30)$$

where $\mathbf{B} = \mathbf{I} + \Delta t M^{-1} \mathbf{A}$ and \mathbf{w} is mean-zero Gaussian with precision $\text{Prec}(\mathbf{w}) = (\sigma \Delta t)^{-2} M$. From this we obtain the block-precision (assuming stationarity)

$$\Lambda_{\mathbf{u}_{(1, \dots, t)}} = \frac{1}{\sigma^2 \Delta t^2} \begin{pmatrix} M & -\mathbf{B}^\top M & \mathbf{0} & \dots & \mathbf{0} \\ -\mathbf{B}^\top M & \mathbf{B}^\top M \mathbf{B} + M & -\mathbf{B}^\top M & \dots & \vdots \\ \mathbf{0} & -\mathbf{B}^\top M & \mathbf{B}^\top M \mathbf{B} + M & \dots & \mathbf{0} \\ \vdots & \vdots & \vdots & \ddots & -\mathbf{B}^\top M \\ \mathbf{0} & \dots & \mathbf{0} & -\mathbf{B}^\top M & M \end{pmatrix}. \quad (31)$$

It is evident that we have Markov properties in time. Spatial Markov properties can also be achieved, attributed to the band-sparsity of \mathbf{A} and a (very common) diagonal approximation of M : While M is band-sparse, the non-zero blocks are generally dense, complicating the spatial Markov structure. By approximating M with its row-sum diagonal, $\tilde{M} = \text{diag}(\sum_j M_{i,j})$, we enforce band-sparsity in the resulting blocks, thereby ensuring spatial Markov properties. This is a common approximation in FEM, which importantly does not increase the error in the solution (Lindgren et al., 2011, Appendix C.5). In the presence of additional sampling error, the importance of the Markov approximation error in using \tilde{M} is further diminished.

Example 5 (FEM solution to Matérn ($\alpha = 2$)). *For the Matérn $\alpha = 2$ we have the SPDE*

$$(\kappa^2 - \text{div } \nabla) \mathbf{u}(\mathbf{x}) = \mathcal{W}(\mathbf{x}) \quad (32)$$

From the Galerkin FEM solution with a linear piecewise basis we obtain the matrices

$$\tilde{M}_{ii} = \sum_{j \in \text{ne}(i)} \int_{\Omega_{ij}} \phi_i(\mathbf{x}) \phi_j(\mathbf{x}) d\mathbf{x} \quad (33)$$

$$A_{ij} = \int_{\Omega_{ij}} \nabla \phi_i(\mathbf{x}) \nabla \phi_j(\mathbf{x}) d\mathbf{x}, \quad (34)$$

where Ω_{ij} represents the union of the mesh elements where the basis functions ϕ_i and ϕ_j overlap. We may then express the precision matrix as:

$$\Lambda_{\mathbf{u}} = \left(\kappa^2 \tilde{M} + \mathbf{A} \right)^\top \tilde{M}^{-1} \left(\kappa^2 \tilde{M} + \mathbf{A} \right). \quad (35)$$

The sparsity of $\Lambda_{\mathbf{u}}$, arising from the sparsity of \mathbf{A} and the diagonal structure of \tilde{M} , demonstrates that \mathbf{u} is a GMRF, as its precision matrix encodes the conditional independence structure of \mathbf{u} .

Both the FDM and FEM approaches lead to sparse precision matrices in the Gaussian case, implying conditional independence and Markov properties. The key driver for this sparsity is the choice of basis functions that are zero almost everywhere over the discretisation/mesh, combined with the locality of the operators L and A .

For more complex (nonlinear and non-Gaussian) variants of (1), the Markov approximation (encoded in Q) to P remains feasible as long as the operators are local. This (parsimonious) approximation is particularly valuable because it reduces the bias $B(\hat{\theta})$ during estimation, and enhances computational efficiency. We will further explore the implications of this approach in the following section, and numerically in Section 6.1.

3.2 Parsimonious Markov Approximation for Filtering

In the filtering problem, we are interested in the distribution of the state u at time t , across the entire spatial domain indexed by \mathbf{x} , but discretised as \mathbf{u}_t . Analysing the solution at a single time point t involves marginalising over all previous time steps. Specifically, integrating over the history,

$$p(\mathbf{u}_t) = \int p(\mathbf{u}_t | \mathbf{u}_{t-1})p(\mathbf{u}_{t-1} | \mathbf{u}_{t-2}) \cdots p(\mathbf{u}_1) d\mathbf{u}_{t-1} \cdots d\mathbf{u}_1 \quad (36)$$

affects the (spatial) Markov properties initially present in the spatio-temporal model. This loss occurs because all spatial points are now indirectly connected through past interactions, which are no longer explicitly conditioned upon.

Distant spatial points require longer temporal paths for connectivity, and the correlation weakens as these paths extend. In simple scenarios, these multiple temporal steps may resemble an AR- k process, where the correlation diminishes exponentially with the number of steps k (see Appendix B). As a result, the marginal distribution may lose strict spatial Markov properties but will likely still exhibit a preference for locality, akin to a "kernel" effect. This is analogous to the fractional Laplacian in Example 4, where global interactions exist, but locality is heavily weighted. This locality preference underlies the effectiveness of distance-based localisation in filtering problems.

From a supervised learning perspective, this locality preference guides models to prioritise local connections, thereby approximating the original spatio-temporal structure. Encoding such an approximation in the parametrisation as Markov properties is, therefore, a logical approach. Indeed, Lindgren et al. (2011) discuss a Markov approximation for the fractional Laplacian, and Lindgren et al. (2022) elaborate further in the context of approximating the exact distribution. In the presence of KLD bias $B(\hat{\theta})$, such a parsimonious approximation becomes even more justifiable.

Section 6.1 experiments numerically with Markov approximations, of increasing order and at increasing ensemble sizes, for the Lorenz-96 (Lorenz, 1995; Lorenz and Emanuel, 1998) filtering problem. It turns out that prioritising local connections is indeed valid.

3.3 Parameter estimation: Independent Sampling, the SPDE Approach, and Bayesian Hierarchical Models

EDA is also employed in typical inverse problems, where the prior is not indexed by time. Instead, the prior consists of static-in-time parameters that are often sampled independently or in groups. For instance, a parameter group might be a spatially indexed vector.

A popular choice for spatial parameter sampling is the Matérn GRF, which may or may not exhibit Markov properties. As discussed in previous sections, random fields defined by Equation (1), can often be well-approximated by assuming Markov properties.

A second class of models with strong structural constraints are Bayesian hierarchical models. Here parameters at one level are treated as random variables with distributions conditioned on parameters at higher levels. The hierarchical structure allows for modelling highly non-Gaussian and complex dependencies, and inference is difficult (Kleppe, 2024). The structure may be encoded as conditional independence represented by a directed acyclic graph $\mathcal{G} = (\mathcal{V}, \mathcal{E})$, in which the edges \mathcal{E} are directed. For the parameters θ in such a model, the joint distribution may be expressed as

$$p(\theta) = \prod_i p(\theta_i | \theta_{\text{pa}(i)}), \quad (37)$$

where $\text{pa}(i)$ are the parents of vertex i in the DAG \mathcal{G} .

The following section discusses how to encode such structure in EDA to achieve good statistical properties while retaining computational and memory efficient computation.

4 An ensemble information filter: Incorporating Markov structure and regularisation in EDA

Common to all the scenarios described in Section 3 is the importance of conditional independence as a meaningful modelling choice encoded in the model Q . This conditional independence can be represented by a graph \mathcal{G} . The remainder of this section develops EDA that estimate prior distributions with respect to \mathcal{G} , enabling easy conditioning on observations.

It is worth noting that the EnKF formulation is not naturally suited for models with conditional independence. The EnKF framework employs a moment parameterisation of the Gaussian, either through the sample covariance matrix or

its square root. To address conditional independence in this parametrisation requires dense matrix inversion, making it difficult to directly encode such properties into the covariance structure.

Instead of encoding this structure in the covariance, we encode conditional independence in the precision $\Lambda_{\mathbf{u}}$ (specifically) and the KR map \mathbf{S} (generally). This encoding of structure aligns with the objective in Equation (16). The complexity and non-linearity of \mathbf{S} , as well as the need for appropriate regularisation, remain open questions. We will further assume that \mathbf{S} is of the affine type, which removes the question of non-linearity and significantly reduces the need for regularisation.

This assumption brings us back to the original goal of this paper: to develop a competitor to the highly successful EnKF. The new method should maintain the computational efficiency and scalability of the EnKF while eliminating the need for manual tuning, such as adaptive or distance-based localisation. However, we believe that tuning the non-linear complexity of \mathbf{S} to the specific problem or data is the next crucial step. Achieving this may lead to fully non-linear, non-Gaussian EDA computations at scale and that is truly adaptive to the problem.

4.1 Encoding conditional independence from \mathcal{G} in the KR-map \mathbf{S}

Conditional independence can be built into \mathbf{S} by considering the inverse KR map

$$\mathbf{S}^{-1}(\mathbf{u}) = \begin{bmatrix} S_1^{-1}(z_1) \\ S_2^{-1}(u_1; z_2) \\ \vdots \\ S_p^{-1}(u_1, \dots, u_{p-1}; z_p) \end{bmatrix} = \begin{bmatrix} u_1 \\ u_2 \\ \vdots \\ u_p \end{bmatrix} = \mathbf{u}, \quad (38)$$

which is evaluated from top to bottom (Ramgraber et al., 2023a,b). Consider conditional independence w.r.t. the AR-1 graph for $p = 4$ (see Figure 9), i.e. $u_3 \perp u_1 | u_2$ and $u_4 \perp u_1, u_2 | u_3$. Then, if the reference p_z factorises to a product distribution (Spantini et al., 2018), writing u_j for redundant arguments and u_j for necessary, we get

$$\mathbf{S}^{-1}(\mathbf{u}) = \begin{bmatrix} S_1^{-1}(z_1) \\ S_2^{-1}(u_1; z_2) \\ S_3^{-1}(u_1, u_2; z_3) \\ S_4^{-1}(u_1, u_2, u_3; z_4) \end{bmatrix} = \begin{bmatrix} u_1 \\ u_2 \\ u_3 \\ u_4 \end{bmatrix} \text{ implies } \begin{matrix} p(u_1) \\ p(u_2 | u_1) \\ p(u_3 | u_1, u_2) \\ p(u_4 | u_1, u_2, u_3) \end{matrix} = \begin{matrix} p(u_1) \\ p(u_2 | u_1) \\ p(u_3 | u_2) \\ p(u_4 | u_3) \end{matrix}. \quad (39)$$

Note that the conditional independence properties mean that u_j is a function only of its neighbours, conditioned on the neighbours being available. The matter of availability implies that the ordering of \mathbf{S} w.r.t. \mathbf{u} is important. It turns out that for telescoping joint distributions, e.g. resulting from Markov properties in time, the optimal ordering is straightforward to find (Ramgraber et al., 2023b). However, for a general graph \mathcal{G} , the question of ordering is more delicate.

Indeed, finding an optimal permutation π that maximises sparsity in the KR-map \mathbf{S} given the conditional independence graph \mathcal{G} , is known to be an NP-hard problem. However, this is a well-researched area, and several algorithms that yield good approximate permutations are available (Cuthill and McKee, 1969; Amestoy et al., 2004; Karypis and Kumar, 1998).

Let \mathbf{S}_π denote the KR-map arranged according to a permutation π (with permutation matrix $\mathbf{\Pi}$), and let $\pi_{\mathcal{G}}$ represent an optimal ordering that minimises the fill-in in the Cholesky decomposition \mathbf{L} of the precision matrix, where $\mathbf{L}\mathbf{L}^\top = \mathbf{\Pi}_{\mathcal{G}}\mathbf{\Lambda}\mathbf{\Pi}_{\mathcal{G}}^\top$. As detailed in Appendix D, by applying the composition of the reverse permutation and the Cholesky-optimised permutation, $\pi_{\mathcal{G}}$, we can derive the KR-map $\mathbf{S}_{\pi_{\mathcal{G}}}$ with significantly reduced sparsity.

This approach ensures that the KR-map $\mathbf{S}_{\pi_{\mathcal{G}}}$ inherits the sparsity benefits of the Cholesky factor \mathbf{L} , allowing us to maintain computational efficiency while encoding most of the conditional independence structure of the model.

4.2 The Ensemble Information Filter

When the transformation \mathbf{S} in the KR-map is affine and the reference measure is Gaussian, the resulting distribution Q is also Gaussian. In this case, Gaussian conditioning is most naturally performed in the canonical parametrisation. The Information Filter (IF) (Kalman and Bucy, 1961; Moore and Anderson, 1979) update equations are well-suited for this, as they operate directly on the precision matrix $\mathbf{\Lambda}$ and the canonical mean $\boldsymbol{\eta} = \mathbf{\Lambda}\boldsymbol{\mu}$. The update equations are:

$$\boldsymbol{\eta}_{t|t} = \boldsymbol{\eta}_{t|t-1} + \mathbf{H}^\top \mathbf{\Lambda}_{\epsilon_t} \mathbf{y}_t, \quad (40)$$

$$\mathbf{\Lambda}_{t|t} = \mathbf{\Lambda}_{t|t-1} + \mathbf{H}^\top \mathbf{\Lambda}_{\epsilon_t} \mathbf{H}, \quad (41)$$

where Λ_{ϵ_t} is the precision of the observation noise ϵ_t . While these equations are mathematically equivalent to the Kalman Filter (KF) (Kalman, 1960) equations, the ensemble approach benefits from the precision matrix because it allows encoding conditional independence structures, thereby minimising divergence bias \mathbf{B} when Λ is estimated from the ensemble.

To implement the IF equations (40) in an Ensemble Information Filter (EnIF), we must adapt them for use with ensemble realisations, which are not explicitly part of the standard equations. Define the canonical realisation as

$$\boldsymbol{\eta}_{t|t-1}^{(i)} = \Lambda_{t|t-1} \mathbf{u}_{t|t-1}^{(i)}, \quad (42)$$

the adjusted sampled observation as

$$\tilde{\mathbf{d}}_t^{(i)} = \mathbf{d} - \mathbf{r}^{(i)}, \quad (43)$$

where $\mathbf{r}^{(i)}$ is the noisy residual defined as

$$\mathbf{r}^{(i)} = \mathbf{h}(\mathbf{u}_{t|t-1}^{(i)}) - \mathbf{H} \mathbf{u}_{t|t-1}^{(i)} + \epsilon, \quad (44)$$

where ϵ is zero-mean Gaussian noise, sampled according to a precision matrix specifying observation uncertainty Λ_{ϵ_t} .

Appendix A demonstrates that the following three steps are equivalent to the EnKF update as described in Example 1 and Example 2:

1. Map realisations to canonical realisations:

$$\boldsymbol{\eta}_{t|t-1}^{(i)} = \Lambda_{t|t-1} \mathbf{u}_{t|t-1}^{(i)}. \quad (45)$$

2. Update each canonical realisation using the IF equations, along with an update of the precision:

$$\boldsymbol{\eta}_{t|t}^{(i)} = \boldsymbol{\eta}_{t|t-1}^{(i)} + \mathbf{H}^\top \Lambda_{\mathbf{r}_t} \tilde{\mathbf{d}}_t^{(i)}, \quad (46)$$

$$\Lambda_{t|t} = \Lambda_{t|t-1} + \mathbf{H}^\top \Lambda_{\mathbf{r}_t} \mathbf{H}. \quad (47)$$

3. Reverse-map each updated canonical realisation to an ordinary updated realisation:

$$\mathbf{u}_{t|t}^{(i)} = \Lambda_{t|t}^{-1} \boldsymbol{\eta}_{t|t}^{(i)}. \quad (48)$$

Thus, if $\Lambda_{t|t-1}$ is estimated from the ensemble of $\mathbf{u}_{t|t-1}$ with respect to the graph \mathcal{G} – which encodes local (conditional independence) structure that is either generated or parsimoniously approximated from the solution to Equation (1) – then the posterior ensemble will suffer significantly less from statistical estimation error, spurious correlations, and ensemble collapse compared to standard EnKFs. This is contingent on \mathbf{H} being either known or estimated with minimal statistical error.

Some important considerations for the EnIF are:

1. **Encoding conditional independence:** The canonical parametrisation is optimal for encoding conditional independence. Section 3 shows how such structures can follow, at least approximately, from a local model (1).
2. **Precision estimation:** For both statistical and computational scalability, $\Lambda_{t|t-1}$ must be efficiently estimated. A well-conditioned SPD result is obtained by estimating Λ through the corresponding affine KR map \mathbf{C} . Only the non-zero elements of a permutation-optimised $\mathbf{C}_{\pi_{\mathcal{G}}}$ should be estimated. This method leverages the row-separation property, making it relatively scalable. However, not all sparsity is retained, and unnecessary degrees of freedom are often introduced.
3. **Locality is intrinsic: adaptive, automatic, and optimal.** Locality is explicitly encoded through estimation with respect to \mathcal{G} . Consequently, the bias \mathbf{B} is expected to be relatively small, eliminating the need for ad-hoc localisation remedies. Since locality is encoded in the parametrisation before estimation, this approach is likely more efficient than traditional post-processing with localising kernels. Furthermore, it will adapt fully to the strength of dependence in the data, requiring no tuning of the "radius of convergence".
4. **Estimating a sparse \mathbf{H} :** The estimation of \mathbf{H} also matters for EnIF's scalability, since it often falls into the $p \gg n$ category. Regularisation is necessary to limit bias \mathbf{B} . Moreover, to maintain sparsity in the posterior precision $\Lambda_{t|t}$, the estimation must produce a sparse result. Algorithms such as the Lasso (Tibshirani, 1996) or Monotone Lasso (Hastie et al., 2007) are natural choices (see Appendix E for details).

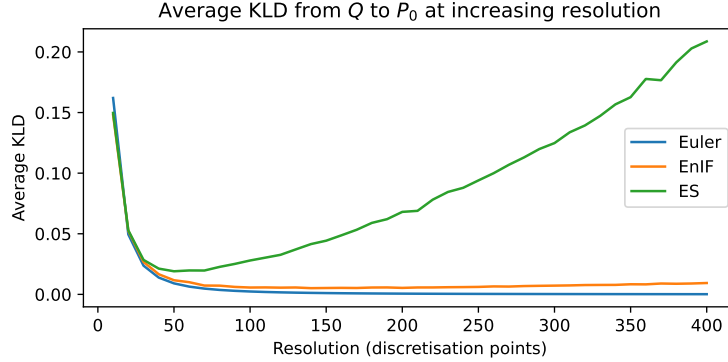


Figure 3: Average KLD values (49) for the EnIF (orange), EnKF/ES (green), and the Euler-Maruyama scheme (blue) relative to the true analytical posterior of the 1D Matérn process ($\kappa = 1.0$) corresponding to the Ornstein-Uhlenbeck process (50). The x -axis shows the level of resolution, indicating the number of discretisation points and thus the number of vertices.

5. **EnKF equivalence under dense estimates:** Estimating Λ using an optimally poor ordering (obtaining a dense result C and Λ), while taking H as the LLS estimator, the EnKF is obtained statistically speaking, but in a computationally inefficient manner.
6. **Statistical efficiency of separating Λ and H estimation:** TMT provides a full likelihood estimation approach for estimating Q . This is done implicitly by placing d first in the block structure of $S_{d,u}$. In EnIF, Q is estimated using a combination of likelihood and regression. This necessitates an efficiency discussion, as divergence bias B depends on the variance of the estimators. The AUMVE property of the full likelihood approach is partially retained. Furthermore, while $\mathbf{y} | \mathbf{u}$ may not be Gaussian, it can be assumed uncorrelated since $\mathbf{y} = g(\mathbf{u})$ is derived from the governing equation. This yields properties close to Gauss-Markov and BLUE, indicating that the regression will be statistically efficient as well.
7. **Smoothing through extending the graph:** Although EnIF is presented as a filtering solution, the smoothing problem can also be addressed by allowing \mathbf{u}_t to include values of the state at times $s \leq t$, with Markov properties in time encoded through \mathcal{G} . For each Monte Carlo simulation, the state vector is appended with new values at time t , as is \mathcal{G} .

5 Synthetic numerical experiments

We now conduct numerical experiments to illustrate the properties of the EnIF. The statistical objective of EDA, as defined in Equation (8), is challenging to evaluate for high-dimensional distributions. However, by selecting examples where both the true distribution P and the approximated distribution Q are multivariate Gaussians, we can use the exact analytical expression for the KLD:

$$D_{\text{KL}}(P||Q) = \frac{1}{2} \left[(\mu_Q - \mu_P)^\top \Sigma^{-1} (\mu_Q - \mu_P) + \text{tr} \left(\Sigma_Q^{-1} \Sigma_P \right) - \log \frac{|\Sigma_P|}{|\Sigma_Q|} - \ln(\mu) \right]. \quad (49)$$

This enables us to evaluate the performance of EnIF under the statistical challenges discussed in Section 2.

5.1 Convergence to the true solution in resolution

Traditional EDA methods often suffer from model divergence as resolution increases, as discussed in Section 2.3. Ideally, higher resolution brings the ensemble distribution P closer to the analytical solution P_0 , which in turn brings the statistical approximation Q closer. This experiment examines whether EnIF may leverage this, and compares it with an EnKF/ES method employing the sample covariance.

To illustrate this, we select a scenario where the distributions of both the analytical solution P_0 and the numerical solution P to Equation (1) are Gaussian. The $n = 1000$ ensemble is generated from P , from which Q in EnIF and ES are estimated.

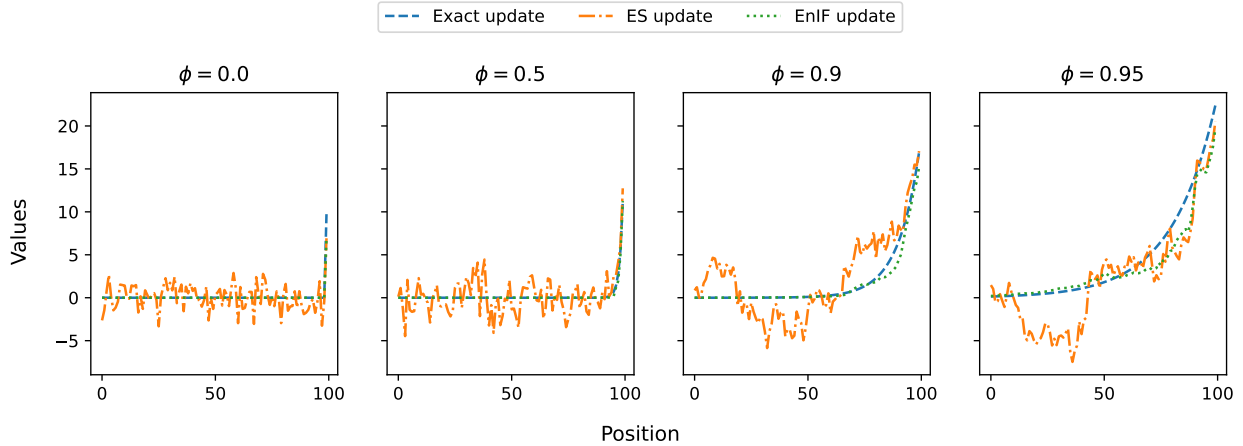


Figure 4: Exact, ES and EnIF updates of the first realisation in an $n = 50$ ensemble of AR-1 processes with varying dependence strength, $\phi \in [0.0, 0.5, 0.9, 0.95]$.

We consider the 1D Matérn process described in Example 1, which corresponds to a specific Ornstein-Uhlenbeck (OU) (Uhlenbeck and Ornstein, 1930) process characterised by the stochastic differential equation

$$dX_t = -\kappa^{-1}X_t dt + dW_t, \quad (50)$$

where W_t is a Wiener process, interpreted in the Itô sense (Øksendal, 2003). The numerical solution P is obtained using the Euler-Maruyama scheme (Kloeden and Platen, 1992), which has strong order of convergence 1.0 for this problem. For the OU process, the Euler scheme reduces to an AR-1 process with $\phi = 1.0 - \kappa^{-1}\Delta t$, leading to a multivariate Gaussian distribution for P , as detailed in Appendix B.

Figure 3 displays the average KLD, $p^{-1}D_{\text{KL}}(P_0||Q)$, where Q is represented by the Euler-Maruyama P or estimated Gaussian distributions from EnIF and EnKF using the ensemble simulated under P .

Initially, both EnKF and EnIF benefit from the reduced divergence from P to P_0 as resolution increases. However, statistical noise in the EnKF quickly dominates, causing the bias term B in Equation (16) to increase, leading Q to diverge from both P and P_0 . In contrast, EnIF closely tracks the Euler scheme, eventually stabilising.

In this experiment, both EnIF and EnKF have parameter spaces that include P , allowing us to analyse the bias term through AIC $B(\theta) = \text{len}(\theta)$. For EnIF, the number of parameters (edges) grows linearly with resolution, resulting in a linear increase in B , which is offset by the averaging over vertices. In comparison, EnKF effectively behaves w.r.t. a fully connected graph, where the number of edges grows quadratically with resolution, causing B to increase quadratically. This leads to a linear growth in the average KLD, as shown by the green line in Figure 3.

5.2 Adapting to strength of dependence

The following experiment verifies that EnIF adaptively adjusts its localisation based on the strength of dependence in the ensemble, as outlined in consideration 3 of Section 4.2.

The AR-1 process (detailed in Appendix B) has Gaussian joint distribution, with its correlation function exhibiting exponential decay. By varying the dependence strength ϕ , we can generate sample paths ranging from independent white noise ($\phi = 0$) to strongly correlated data ($\phi \rightarrow 1$). We examine ensembles with $p = 100$ steps and a relatively small ensemble size $n = 50$ to make the statistical estimation effects more visible.

For each experiment, we assimilate an observation of the endpoint $d = 20$, with a standard normal observation noise. This observation, chosen far from the prior, combined with small observation noise, increases the innovation term of the Kalman filter. This will highlight statistical inconsistencies, making them easier to observe.

In Figure 4 we compare updates from the exact solution, EnIF, and EnKF/ES, across different values of ϕ ($\phi \in [0.0, 0.5, 0.9, 0.95]$).

The EnKF/ES update shows significant unwanted random behaviour, especially when dependence is weak. For instance, in the left-most panel ($\phi = 0$), where there is no true correlation, the exact solution only updates the last value, while the rest of the state retains the prior. In contrast, EnKF/ES updates all values noisily, introducing unnecessary variations where no correlation exists.

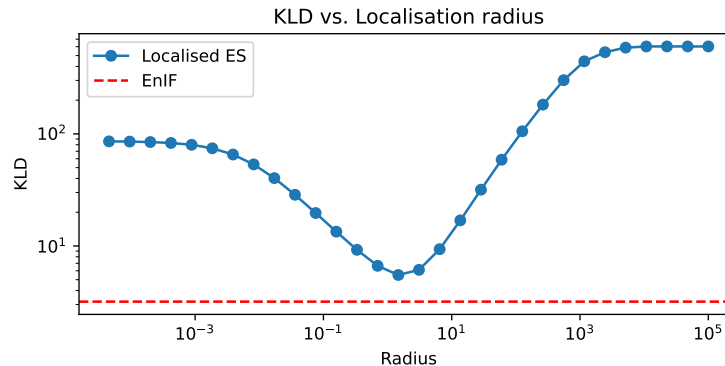


Figure 5: KLD values (49) vs. localisation radius of ES/EnKF. Both the x - and y -axes are on a log-scale.

EnIF, by contrast, demonstrates a built-in adaptive localisation due to the use of the graph \mathcal{G} . Regardless of the dependence strength, EnIF provides smoother and more reliable updates, closely tracking the exact solution. While not entirely free from statistical error, EnIF's updates are consistently more accurate, especially at points of weak dependence and smaller updates.

In all cases, EnIF's deviations from the exact update are minimal, demonstrating its ability to automatically adapt to varying strengths of dependence without requiring manual tuning, unlike traditional localisation methods.

5.3 Implicit optimal localisation

In the previous subsection, we demonstrated that ES/EnKF requires something to mitigate spurious correlations. In practice, most ES and EnKF-type methods employ some form of localisation, which, while ad-hoc and lacking theoretical justification, greatly improves their performance. To provide a meaningful comparison, it is necessary to compare EnIF with a localised ES/EnKF.

We consider the same Matérn model and experimental setup as in Section 5.1, focusing on the highest resolution example with $p = 1000$ and a large ensemble size of $n = 1000$ to minimise the effect of statistical errors. With a fixed \mathbf{H} , we use covariance localisation (Houtekamer and Mitchell, 2001), varying the radius of influence c from small to large. We then compare the localised ES/EnKF statistical model Q to the true solution P_0 using the Gaussian KLD (49) across different values of c , and also compute the KLD to P_0 for the EnIF statistical model Q .

Figure 5 presents the results. At very small values of c , the localisation effect is negligible, and Q behaves like the vanilla ES/EnKF. As c increases, the localisation effect improves the KLD, reaching an optimal value for the localised ES (blue line). However, further increases in c weaken the updates too much, eventually reducing the covariance matrix to a diagonal structure with only sample variances. Across all values of c , EnIF achieves a lower KLD.

EnIF inherently encodes how information should propagate through the system. In models governed by local operators, such as those described by Equation (1), information cannot "teleport" across distant state variables – it must propagate through the system. EnIF captures this through its Markov properties, which restrict the degrees of freedom during estimation, thereby minimising B and focusing on relevant regions in the space of covariance matrices. In contrast, the ES/EnKF methods allow information to propagate unrealistically, and while localisation dampens this effect, it remains suboptimal because the structure should ideally be imposed before any statistical estimation occurs.

6 Applications to smoothing, filtering, and parameter estimation

This chapter demonstrates how EnIF can be applied in diverse settings, including filtering, smoothing, and parameter estimation. We also explore how to obtain structure and Markov graphs for these problems.

6.1 Filtering: Lorenz-96 dynamics with Runge-Kutta-4 integration

The Lorenz-96 model (Lorenz, 1995; Lorenz and Emanuel, 1998) is a deterministic dynamical system describing the m -dimensional state variable $\mathbf{x}(t)$, evolving as:

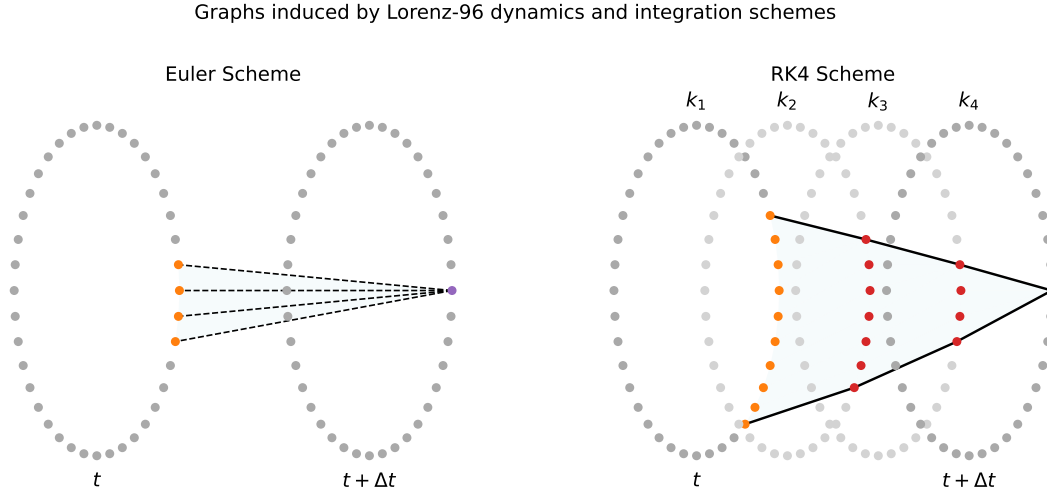


Figure 6: Conditional independence graphs induced by integrating the Lorenz-96 dynamics (with 40 states) in Equation (51) using the Euler scheme (left) and the RK4 scheme (right).

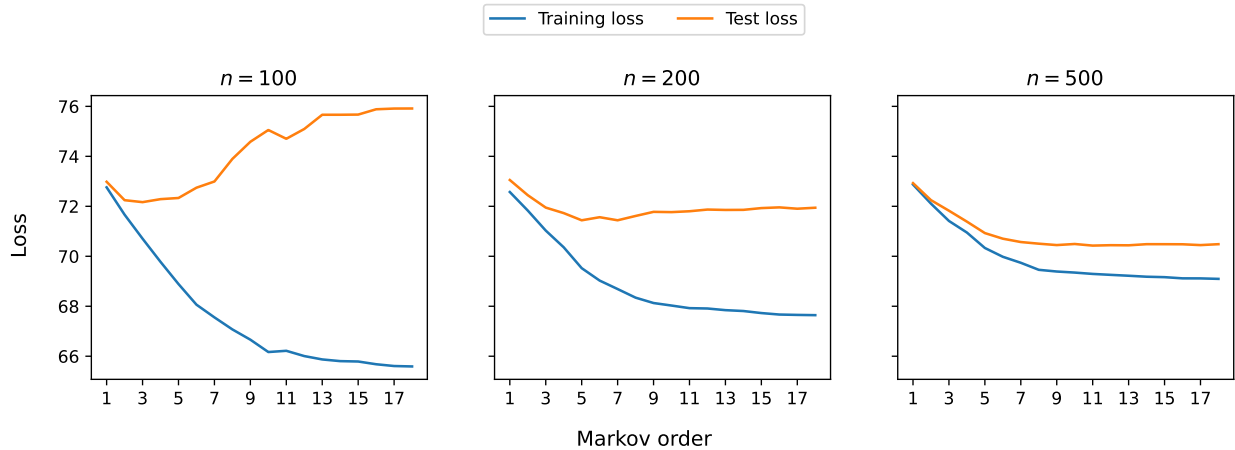


Figure 7: Negative log-likelihood loss versus Markov order for the Lorenz-96 filtering problem. Loss is computed for training and test sets of size $n \in [100, 200, 500]$.

$$\frac{d}{dt}x_j = (x_{j+1} - x_{j-2})x_{j-1} - x_j + F, \tag{51}$$

where $x_{-1} = x_{m-1}$, $x_0 = x_m$, $x_{m+1} = x_1$, and $m \geq 4$ (here $m = 40$). The constant forcing term $F = 8$ generates chaotic dynamics.

The Lorenz-96 model is a standard benchmark in EDA literature. We follow a similar setup to Ramgraber et al. (2023b), initializing $\mathbf{x}_0 \sim 0.01\mathbf{z}$, where \mathbf{z} is standard Gaussian. Using the Runge-Kutta 4 (RK4) scheme, the system is integrated up to $t = 4.0$, generating training and test sets of size $n \in [100, 200, 500]$.

The conditional independence graphs induced by integrating Equation (51) using the Euler and RK4 schemes differ. For a visual reference, see Figure 6. The Euler scheme connects $\mathbf{x}_j(t + \Delta t)$ with $\mathbf{x}_{j-2}(t)$, $\mathbf{x}_{j-1}(t)$, $\mathbf{x}_j(t)$, and $\mathbf{x}_{j+1}(t)$, while the RK4 scheme incorporates longer-range dependencies, connecting $j - 6$ through $j + 3$. For smoothing, estimating Λ using the RK4 graph ensures all relevant connections are included. However, at smaller sample sizes, restricting Λ to the simpler Euler graph can reduce statistical noise.

For filtering, no nodes are truly conditionally independent. Following Section 3.2, we construct a parsimonious circular graph where node j connects only to $j - 1$ and $j + 1$. The Markov order is then incrementally increased by including

neighbors' neighbors, and the loss (Equation (14)) is evaluated on training and test sets. The evaluations are presented in Figure 7.

The results align with the theoretical predictions of Section 3.2. The optimal Markov order, minimising test loss, increases with sample size, reaching approximately 2, 5, and 7 for $n = 100$, $n = 200$, and $n = 500$, respectively. At infinite ensemble size, a fully connected graph (as in the EnKF) would be correct, but finite ensembles require avoiding overfitting. By leveraging the induced local kernel effect in filtering, EnIF effectively balances parsimony and model accuracy.

6.2 Smoothing: Stochastic heat-equation and Precision Equation (31)

We now showcase explicit usage of Equation (31) using the 2D stochastic heat equation:

$$\frac{\partial u}{\partial t} - \alpha \operatorname{div} \nabla u = \sigma \mathcal{W}, \quad (52)$$

where $u_t(\mathbf{x})$ is the temperature, $\mathbf{x} = (x_1, x_2)$ is the spatial position, α is the thermal diffusivity, and $\sigma \mathcal{W}$ represents white noise. The spatial domain Ω is discretised using a triangular mesh, dividing it into elements T_e over which basis functions ϕ_i are defined. We approximate $u(\mathbf{x}, t)$ by values at the mesh vertices.

The solution requires constructing the matrices \mathbf{M} and \mathbf{A} given by Equation (25). Each entry M_{ij} and A_{ij} is computed as a sum over the contributions of local elements T_e , which belong to Ω_{ij} :

$$M_{ij} = \sum_{e \in \Omega_{ij}} \int_{T_e} \phi_i(\mathbf{x}) \phi_j(\mathbf{x}) d\mathbf{x}, \quad (53)$$

$$A_{ij} = \sum_{e \in \Omega_{ij}} \int_{T_e} \alpha \nabla \phi_i(\mathbf{x}) \cdot \nabla \phi_j(\mathbf{x}) d\mathbf{x}. \quad (54)$$

For linear basis functions, the local mass matrix over T_e evaluates to:

$$M^{(e)} = \frac{\operatorname{Area}(T_e)}{12} \begin{pmatrix} 2 & 1 & 1 \\ 1 & 2 & 1 \\ 1 & 1 & 2 \end{pmatrix}, \quad (55)$$

with the Markov approximation:

$$\tilde{M}^{(e)} = \frac{\operatorname{Area}(T_e)}{3} \mathbf{I}_3. \quad (56)$$

The local stiffness matrix represents the Laplacian term and starts as:

$$A_{ij}^{(e)} = \int_{T_e} \alpha \phi_j(\mathbf{x}) \operatorname{div} \nabla \phi_i(\mathbf{x}) d\mathbf{x}.$$

Applying integration by parts to reduce the Laplacian to first-order derivatives, and assuming boundary terms vanish, this becomes:

$$A_{ij}^{(e)} = \int_{T_e} \alpha \nabla \phi_j(\mathbf{x}) \cdot \nabla \phi_i(\mathbf{x}) d\mathbf{x}.$$

For a triangular element T_e with vertices $(x_{1,1}, x_{1,2})$, $(x_{2,1}, x_{2,2})$, and $(x_{3,1}, x_{3,2})$, the gradients of the basis functions ϕ_i are constant and given by:

$$\nabla \phi_i = \begin{pmatrix} b_i \\ c_i \end{pmatrix}, \quad b_i = \frac{x_{j,2} - x_{k,2}}{2\operatorname{Area}(T_e)}, \quad c_i = \frac{x_{k,1} - x_{j,1}}{2\operatorname{Area}(T_e)}, \quad (57)$$

where (i, j, k) are cyclic permutations of the triangle vertices. The local stiffness matrix is then:

$$A^{(e)} = \frac{\alpha}{4\operatorname{Area}(T_e)} \begin{pmatrix} b_1^2 + c_1^2 & b_1 b_2 + c_1 c_2 & b_1 b_3 + c_1 c_3 \\ b_2 b_1 + c_2 c_1 & b_2^2 + c_2^2 & b_2 b_3 + c_2 c_3 \\ b_3 b_1 + c_3 c_1 & b_3 b_2 + c_3 c_2 & b_3^2 + c_3^2 \end{pmatrix}. \quad (58)$$

The global matrices \mathbf{M} and \mathbf{A} are assembled by summing contributions from all triangular elements T_e in the domain Ω . These matrices are sparse, with non-zero entries only for neighbouring vertices in the mesh. The precision of \mathbf{u}_t in Equation (31) retains this sparsity as long as the diagonal approximation $\tilde{\mathbf{M}}$ is used.

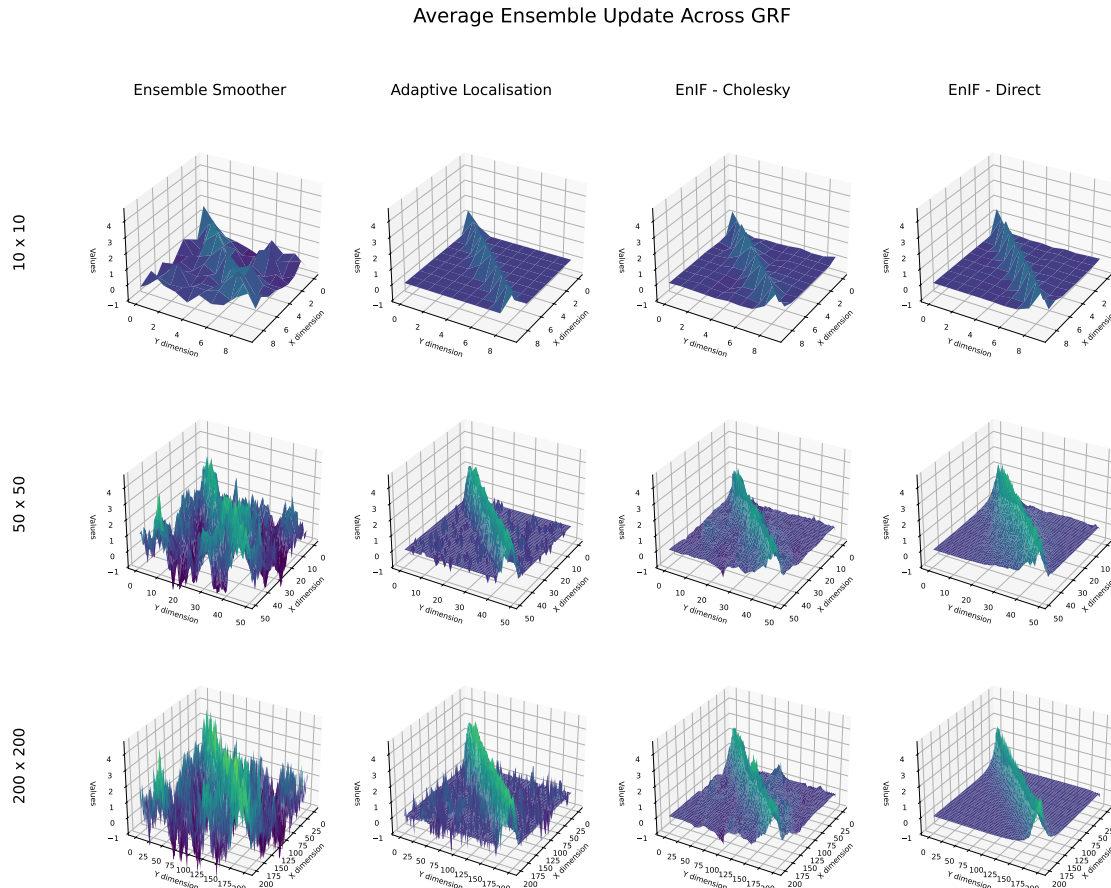


Figure 8: The average ($n = 100$) ensemble update across the GRFs at varying discretisation, using different update algorithms. The GRFs are sampled using an anisotropic exponential covariance function. This is a special case of the Matérn covariance, which in the case of two dimensions does not yield a Markov property. The response is sampled as $y = u + z$ for $z \sim \mathcal{N}(0, 0.1^2)$, i.e. direct but noisy observations across the diagonal elements in u . Thus the true \mathbf{H} is sparse, but is here assumed unknown. The updates depend on estimated quantities.

6.3 Static parameters: Large 2D Anisotropic Exponential (non Markovian) GRF

EDA is widely used in history matching within reservoir engineering. Algorithms like the ES and ES-MDA (Emerick and Reynolds, 2013) are popular for updating ensembles of parameters representing geological uncertainty. This uncertainty is often modeled using GRFs (Sebacher et al., 2017). Here, we illustrate how EnIF addresses the challenges of high-dimensional parameter estimation in such settings.

We sample $n = 100$ 2D GRFs with an anisotropic exponential covariance function. The exponential is a special case of Matérn, but does not exhibit Markov properties in two dimensions. The GRFs are sampled at three discretisation levels: 10×10 , 50×50 , and 200×200 , corresponding to 100, 2,500, and 40,000 parameters, respectively. The response is modelled as $y = u + z$, where $z \sim \mathcal{N}(0, 0.1^2)$, representing direct but noisy observations along the diagonal elements in u . The true population \mathbf{H} is sparse, consisting of zeros and ones, but this structure is not provided to the algorithms. Instead, \mathbf{H} must be implicitly or explicitly estimated. In practical history matching applications, \mathbf{h} is both unknown and non-linear, and thus the population \mathbf{H} is subject to residual errors. Here modeled by z . Finally, we assume additional observation variance of 1.0.

We evaluate updates from four methods:

1. ES.
2. ES with Adaptive Localisation using a threshold $3\sqrt{n}^{-1}$ (see red-lines in Figure 2).
3. EnIF with precision estimated via a permutation-optimised affine KR-map (approximately a Cholesky factor)
- 4.1.

4. EnIF with a directly estimated precision matrix (Lunde et al., 2022).

The average updates, computed as $n^{-1} \sum_i (\mathbf{u}_{t|t}^{(i)} - \mathbf{u}_{t|t-1}^{(i)})$, are shown in Figure 8.

Increasing resolution amplifies the statistical challenges described in Section 2.3. At 200×200 (40,000 parameters), the ES update fails to distinguish noise from signal, resulting in erratic updates. Adaptive localisation mitigates this issue but lacks an intrinsic preference for locality. Consequently, we observe random spikes and strong updates far from the diagonal.

In contrast, EnIF updates are significantly more localised, even at high resolution. However, the Cholesky variant exhibits a slightly "tweaky" behaviour due to the extra degrees of freedom introduced by in-fill. The direct estimation method avoids this issue but sacrifices some efficiency in parameter estimates and may require a higher Markov order. Additionally, ensuring a SPD estimate is non-trivial for sparsity-aware direct methods.

A thorough discussion of precision estimation for extremely high-dimensional problems is beyond the scope of this paper, but it remains a critical area for ensuring EnIF's scalability to even larger systems.

Similarly, estimating \mathbf{H} efficiently is a significant regression challenge, deserving of a separate discussion. We have implemented an efficient boosting-type algorithm with linear base-learners and automatic stopping. It is particularly well-suited for high-dimensional problems. For full details and the accompanying pseudo-algorithm, refer to Appendix E and its implementation in <https://github.com/equinor/graphite-maps>.

The ES-MDA algorithm is a standard approach for addressing the non-linearity of \mathbf{h} , applying the ES iteratively over multiple steps. Similarly, EnIF can be extended to a multi-iteration framework, referred to as EnIF-MDA. In Appendix F, we replicate the proofs for ES-MDA, demonstrating their equivalence in the linear case, but using the canonical parametrisation for simplified linear algebra.

7 Discussion

This paper addresses the statistical challenges inherent in EDA, particularly the reliance on localisation to mitigate issues such as spurious correlations and ensemble collapse. By integrating theory from triangular measure transport, supervised learning, and SPDEs, we propose leveraging Markov properties as a robust solution. EnIF is introduced as a direct competitor to the celebrated EnKF and ES, encoding Markov properties through sparsity. Numerical experiments were designed to showcase EnIF's specific advantages, including convergence, adaptiveness, and optimality, and the methodology was demonstrated across filtering, smoothing, and parameter estimation tasks—each relevant to different fields of study.

EnIF eliminates the need for localisation during updates. Spurious correlations and ensemble collapse are managed implicitly through its improved statistical properties, offering a clear advantage over traditional approaches like the EnKF.

The methodology is user-friendly for practitioners. Its requirements are minimal: practitioners need only supply the standard state/parameter and response matrices, along with a graph specifying conditional independence in the state/parameter matrix. EnIF is also highly scalable, both statistically and computationally.

Promising avenues for future research include enabling the estimated KR-map to incorporate non-linear map components while maintaining the adaptiveness and scalability of EnIF. Additionally, the underlying statistical learning algorithms—specifically the sparse regression for responses onto states/parameters and the precision estimation—could be refined to further enhance stability and scalability. In particular, for extremely large scale applications, estimation employing either the computational graph of \mathbf{h} , or weighted regression techniques employing knowledge of position, might be necessary to overcome difficult signal-to-noise ratios.

A Information filter update equivalent to Kalman update

The Ensemble Kalman filter update equation is

$$\mathbf{u}_{t|t}^{(i)} = \mathbf{u}_{t|t-1}^{(i)} + \mathbf{K}(\mathbf{d}_t - \mathbf{d}_{t|t-1}^{(i)}) = \mathbf{u}_{t|t-1}^{(i)} + \mathbf{K}(\mathbf{d}_t - (\mathbf{y}_{t|t-1}^{(i)} + \boldsymbol{\epsilon}^{(i)})) \quad (59)$$

where the Kalman gain is

$$\mathbf{K} = \boldsymbol{\Sigma}_{\mathbf{u}\mathbf{y}} \boldsymbol{\Sigma}_{\mathbf{d}}^{-1} = \boldsymbol{\Sigma}_{t|t-1} \mathbf{H}^\top (\boldsymbol{\Sigma}_{\mathbf{y}} + \boldsymbol{\Sigma}_{\boldsymbol{\epsilon}})^{-1}. \quad (60)$$

In the following we show how to produce the same update but through the Information filter update equation. The Ensemble Information filter update is

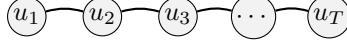


Figure 9: The graph corresponding to an AR-1 process

- Rescale each realisation into the "canonical" space

$$\boldsymbol{\eta}_{t|t-1}^{(i)} = \Lambda_{t|t-1} \mathbf{u}_{t|t-1}^{(i)}. \quad (61)$$

- Update each rescaled realisation using the IF equations, along with an update of the precision

$$\boldsymbol{\eta}_{t|t}^{(i)} = \boldsymbol{\eta}_{t|t-1}^{(i)} + \mathbf{H}^\top \Lambda_{\mathbf{r}_t} \tilde{\mathbf{d}}_t^{(i)} \quad (62)$$

$$\Lambda_{t|t} = \Lambda_{t|t-1} + \mathbf{H}^\top \Lambda_{\mathbf{r}_t} \mathbf{H}. \quad (63)$$

- Bring each rescaled realisation back to its original space

$$\mathbf{u}_{t|t}^{(i)} = \Lambda_{t|t}^{-1} \boldsymbol{\eta}_{t|t}^{(i)}. \quad (64)$$

To see that the Kalman update is the same as the Information filter update, note firstly that

$$\begin{aligned} \Lambda_{t|t}^{-1} \boldsymbol{\eta}_{t|t-1}^{(i)} &= \Lambda_{t|t}^{-1} \Lambda_{t|t-1} \mathbf{u}_{t|t-1}^{(i)} \\ &= (\Sigma_{t|t-1} - \mathbf{K} \mathbf{H} \Sigma_{t|t-1}) \Sigma_{t|t-1}^{-1} \mathbf{u}_{t|t-1}^{(i)} \\ &= \mathbf{u}_{t|t-1}^{(i)} - \mathbf{K} \hat{\mathbf{y}}_{t|t-1}^{(i)}, \end{aligned} \quad (65)$$

where $\hat{\mathbf{y}}_{t|t-1}^{(i)} = \mathbf{H} \mathbf{u}_{t|t-1}^{(i)}$. Secondly, note that $\mathbf{K} = \Sigma_{t|t} \mathbf{H}^\top \Lambda_{\mathbf{r}_t}$ from an application of Woodbury matrix inversion formula (see e.g. Moore and Anderson (1979)). Therefore

$$\Lambda_{t|t}^{-1} \mathbf{H}^\top \Lambda_{\mathbf{r}_t} \tilde{\mathbf{d}}_t^{(i)} = \mathbf{K} \tilde{\mathbf{d}}_t^{(i)}. \quad (66)$$

Define the noisy residual as $\mathbf{r}^{(i)} = \mathbf{h}(\mathbf{u}_{t|t-1}^{(i)}) - \mathbf{H} \mathbf{u}_{t|t-1}^{(i)} + \boldsymbol{\epsilon}$, where $\boldsymbol{\epsilon}$ is zero-mean Gaussian noise ϵ_t sampled according to a precision specifying observation uncertainty Λ_{ϵ_t} . Thus $\Lambda_{\mathbf{r}_t}$ specifies all uncertainty in a prior simulation of the uncertain observation $\tilde{\mathbf{d}}_{t|t-1}^{(i)} = \mathbf{h}(\mathbf{u}_{t|t-1}^{(i)}) + \boldsymbol{\epsilon}^{(i)}$ not explained by the regression $\mathbf{H} \mathbf{u}_{t|t-1}^{(i)}$. Finally, let $\tilde{\mathbf{d}}_t^{(i)} = \mathbf{d} - \mathbf{r}^{(i)}$. Then we see that

$$\begin{aligned} \Lambda_{t|t}^{-1} \boldsymbol{\eta}_{t|t}^{(i)} &= \Lambda_{t|t}^{-1} \left(\boldsymbol{\eta}_{t|t-1}^{(i)} + \mathbf{H}^\top \Lambda_{\mathbf{r}_t} \tilde{\mathbf{d}}_t^{(i)} \right) \\ &= \mathbf{u}_{t|t-1}^{(i)} - \mathbf{K} \hat{\mathbf{y}}_{t|t-1}^{(i)} + \mathbf{K} \tilde{\mathbf{d}}_t^{(i)} \\ &= \mathbf{u}_{t|t-1}^{(i)} + \mathbf{K} \left(\mathbf{d} - (\mathbf{h}(\mathbf{u}_{t|t-1}^{(i)}) + \boldsymbol{\epsilon}^{(i)}) \right) \\ &= \mathbf{u}_{t|t}^{(i)}. \end{aligned} \quad (67)$$

B The AR-1 process

The AR-1 process is defined by

$$u_t = \phi u_{t-1} + \epsilon_t, \quad u_1 \sim \mathcal{N}\left(0, \frac{1}{1-\phi^2}\right), \quad \epsilon_t \sim \mathcal{N}(0, 1). \quad (68)$$

Here, some u_t is "generated" only by u_{t-1} , implying a first order connection formalised as edges only between sequential elements as shown in Figure 9. Correspondingly, the precision matrix of $\mathbf{u} = [u_1, \dots, u_T]^\top$ is tridiagonal and sparse, in contrast to the dense covariance

$$\Sigma_{\mathbf{u}} = \begin{bmatrix} B(1,1) & \cdots & B(1,T) \\ \vdots & \ddots & \vdots \\ B(T,1) & \cdots & B(T,T) \end{bmatrix}, \quad B(i,j) = \frac{\phi^{|i-j|}}{1-\phi^2}, \quad \Lambda_{\mathbf{u}} = \begin{bmatrix} 1 & -\phi & & & \\ -\phi & 1+\phi^2 & -\phi & & \\ & \ddots & \ddots & \ddots & \\ & & -\phi & 1+\phi^2 & -\phi \\ & & & -\phi & 1 \end{bmatrix} \quad (69)$$

formed by considering that u_t depends upon u_{t-1} which depends upon u_{t-2} and so on.

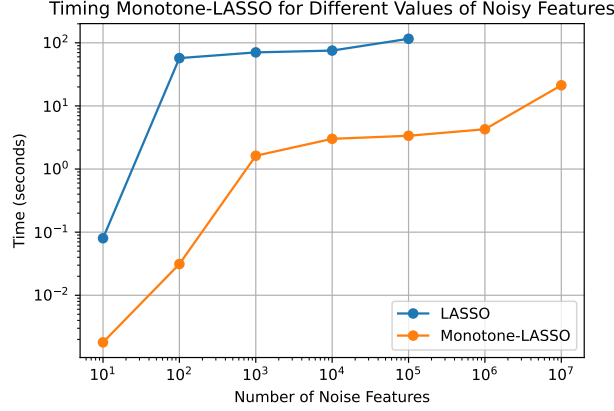


Figure 10: Timing LASSO from the python package sklearn and the Monotone LASSO in Algorithm 1, versus an increasing number of (noisy) regression features.

C The Matérn-1/Ornstein-Uhlenbeck analytical and approximate solutions

The OU SDE in Equation (50) correspond to the specific 1D Matérn SPDE in Equation (2) with $\kappa = 1.0$. Therefore, the stationary covariance between time-points Δt is $\frac{1}{2}e^{-\Delta t}$.

When integrated approximately using the Euler-Maruyama scheme, the process follows the AR-1 dynamics in Appendix B, with $\phi = 1 - \Delta t$.

D Applying fill-in reduction algorithms on $C^\top C = \Lambda$

We have that C is lower triangular and that $\Lambda_u = C^\top C$. In-fill reduction algorithms like the AMD ordering (Amestoy et al., 2004), Reverse-Cuthill McKee ordering (Cuthill and McKee, 1969), or METIS (Karypis and Kumar, 1998) are typically implemented for the ordinary Cholesky decomposition $\Lambda = LL^\top$ where L also is lower triangular. We seek to exploit these algorithms for finding an ordering π of u so that $C(\pi)$ has as little in-fill as possible compared to that of Λ_u .

First, note that the Cholesky decomposition is unique because Λ_u is positive definite. Let P_r be the symmetric permutation matrix reversing the order, $\pi_r = (p, \dots, 1)$, then $P_r = P_r^\top = P_r^{-1}$ and $P_r P_r = I$. We have that

$$P_r \Lambda_u P_r = (P_r C^\top P_r)(P_r C^\top P_r)^\top. \quad (70)$$

Thus from uniqueness $P_r C^\top P_r = \tilde{L}$ must be a lower triangular Cholesky factor of the reversed precision $\hat{\Lambda}_u = P_r \Lambda_u P_r$, since this too is SPD. Note that \tilde{L} will have the same amount of in-fill as C , as the reverse permutation changes nothing here. Therefore, we may first seek an additional optimised permutation, say P_* , so that the Cholesky factor, say L_* , has as little extra non-zeroes compared to Λ_u as possible. As such, seek an optimized ordering P_* and corresponding sparsity structure of a Cholesky factor L_* as

$$L_* L_*^\top = P_*^\top \Lambda_u P_*. \quad (71)$$

We may then find the sparsity structure of $C(\pi^*)$ from using (70):

$$C(\pi^*) = (P_r L_* P_r)^\top. \quad (72)$$

The elements of $C(\pi^*)$ may then be learned from data optimising (9) only w.r.t. the non-zero elements of $C(\pi^*)$. To "unwrap" and retrieve the original precision, we may calculate it as

$$\Lambda_u = P_* P_r C(\pi^*)^\top C(\pi^*) P_r P_*^\top. \quad (73)$$

E Fast regularised sparse regression through boosting with linear base learners

Raanes et al. (2023) connects the "average sensitivity" of the estimated H in EnKF-type methods with the expected gradient, $\mathbb{E}[\nabla h(u)]$, when $n \rightarrow \infty$. Thus the population estimate is indeed the expected gradient. We now describe the

underlying elements to Algorithm 1, which may be used when \mathbf{H} is unknown and the dimension of \mathbf{u} is large. It was used to produce the results in Section 6.3.

We estimate \mathbf{H} row-by-row. Thus, it is sufficient to consider only a vector of responses \mathbf{y} , and regression coefficients β eventually inserted as the row. We thus assume \mathbf{H} is $1 \times p$ in the following.

First, the data-matrix $\mathbf{U} = [\mathbf{u}^{(1)} \dots \mathbf{u}^{(n)}]^\top$ is standardised. This is to ensure features are comparable at the same scale, and weighted equally by regularisation, see e.g. Hastie et al. (2009) and the LASSO. The response vector is also standardised, but for numerical reasons. This means that estimated coefficients $\hat{\beta}_j$ needs a rescaling before insertion into \mathbf{H} , i.e. $\hat{\mathbf{H}}_{1,j} = \hat{\sigma}_y \hat{\sigma}_{u_j}^{-1} \hat{\beta}_j$.

To retain sparsity of the posterior precision, $\Lambda_{t|t}$, it is important to seek a sparse estimate $\hat{\mathbf{H}}$. However, for statistical estimation reasons we could have chosen e.g. Ridge regression (Hoerl and Kennard, 1970) yielding a dense estimate. Note however also the "always bet on sparsity" principle (Hastie et al., 2009), and the added explainability element of how certain responses effects only a few state-elements directly.

The go-to sparse linear regression algorithm is the LASSO (Tibshirani, 1996). There are efficient coordinate descent algorithms for solving the optimisation problem, but unfortunately, seemingly too slow for large problems like in Section 6.3 with multiple responses. See Figure 10 for some timing experiments.

Instead we implement a version of the Monotone-LASSO (Hastie et al., 2007). This may be seen as a form of boosting (Friedman, 2001; Mason et al., 1999) with 1D linear base learners. To make it adaptive and computationally efficient, we implement early stopping using an approximation of n -fold cross-validation (Stone, 1974; Claeskens and Hjort, 2008). The algorithm is provided in Algorithm 1, and implemented in pure Python here <https://github.com/equinor/graphite-maps>.

Figure 10 shows significant speed-ups compared to the standard LASSO. Furthermore the additional regularisation is beneficial for large scale applications: For the medium 50×50 2D GRF example in Section 6.3, the LASSO (tuned with 10-fold cross validation) produces 1255 non-zero elements in its estimate of \mathbf{H} , while the monotone LASSO produces only 50 non-zeroes. The population quantity has 50, while a dense estimate contains 125,000 elements.

Finally, if the signal-to-noise ratio cannot be overcome by ordinary (uninformed) regression, it might be beneficial to either utilise the computational graph (see e.g. Kristensen et al. (2016)) or knowledge regarding positions of \mathbf{u} and \mathbf{y} for use in weighted boosting regression.

Algorithm 1 Monotone LASSO with information-theoretic early stopping

Input:

- An $n \times p$ matrix of standardised feature realisations \mathbf{X}
- An n -vector of response realisations \mathbf{y}

Do:

1. **Initialise** $\hat{\beta}_0 = \mathbf{0}$
2. **While** $\text{mse}_{cv-n}(\mathbf{X}, \mathbf{y}; \hat{\beta}_k) > \text{mse}_{cv-n}(\mathbf{X}, \mathbf{y}; \hat{\beta}_{k+1})$:
 - i) Calculate all 1D linear regressions
 - ii) Select β_j as the one reducing training mse the most
 - iii) $\hat{\beta}_{k+1,j} = \hat{\beta}_{k,j} + \epsilon \beta_j$**end While**
3. **Return** $\hat{\beta}$.

Notes:

- $cv-n$ is computed using $\hat{\theta}_{-i} \xrightarrow{n} \hat{\theta} - n^{-1} \text{IF}(y_i, \mathbf{x}_i)$, where the influence IF is found using the asymptotic properties of $\hat{\beta}_j$ as an M-estimator. See $cv-n$ and TIC relation through IF in Claeskens and Hjort (2008).
- For these 1D regressions, we construct the estimate

$$\text{IF}(y^{(i)}, \mathbf{x}_j^{(i)}) = - \left(y^{(i)} - \hat{\beta}_j \mathbf{x}_j^{(i)} \right) \mathbf{x}_j^{(i)} \left[-n^{-1} \sum_i (\mathbf{x}_j^{(i)})^2 \right]^{-1}$$

F On the multiple-data-assimilation extension

We establish that EnIF may be used within as EnIF-MDA by repeating the Gaussian-linear proof of Emerick and Reynolds (2013) using the precision. This also shows that the canonical parametrisation is "natural" for conditioning a Gaussian, as the derivations here are rather straightforward. Appendix A showcase the equivalence of EnKF and EnIF when the covariance/precision and \mathbf{H} are known. This may also be considered as the infinite ensemble case. Furthermore, EnIF is different in the sense that it directly updates the precision matrix. We therefore only need to show that the EnIF-MDA updated precision is equivalent to the EnIF updated precision under linear Gaussian dynamics.

Let $\mathbf{\Lambda}_{t|t-1}$ be the ordinary prior precision. $\mathbf{\Lambda}_r = \mathbf{\Lambda}_\epsilon$ is the ordinary measurement uncertainty, note that $\mathbf{h}(\mathbf{u}) = \mathbf{H}\mathbf{u}$ and that we therefore have equivalence. We then define the equivalent MDA quantities as

$$\tilde{\mathbf{\Lambda}}_\epsilon = \begin{bmatrix} \alpha_1 \mathbf{\Lambda}_\epsilon & \mathbf{0} & & & \\ \mathbf{0} & \alpha_2 \mathbf{\Lambda}_\epsilon & & & \\ & & \ddots & & \\ & & & \alpha_{K-1} \mathbf{\Lambda}_\epsilon & \\ & & & \mathbf{0} & \alpha_K \mathbf{\Lambda}_\epsilon \end{bmatrix} \text{ and } \tilde{\mathbf{H}} = \begin{bmatrix} \mathbf{H} \\ \vdots \\ \mathbf{H} \end{bmatrix} \quad (74)$$

where $\sum_{k=1}^K \alpha_k = 1$, and we assume K iterations.

From direct calculation, we obtain that the EnIF-MDA precision is equivalent to the EnIF updated precision:

$$\begin{aligned} \tilde{\mathbf{\Lambda}}_{t|t} &= \mathbf{\Lambda}_{t|t-1} + \tilde{\mathbf{H}}^\top \tilde{\mathbf{\Lambda}}_\epsilon \tilde{\mathbf{H}} \\ &= \mathbf{\Lambda}_{t|t-1} + \sum_{k=1}^K \alpha_k \mathbf{H}^\top \mathbf{\Lambda}_\epsilon \mathbf{H} \\ &= \mathbf{\Lambda}_{t|t-1} + \mathbf{H}^\top \mathbf{\Lambda}_\epsilon \mathbf{H} \\ &= \mathbf{\Lambda}_{t|t}. \end{aligned} \quad (75)$$

Acknowledgments

I would like to thank Gilson Moura Silva Neto, Max Ramgraber, Tommy Odland, and Tore Kleppe for their valuable feedback on early versions of this paper. Their insights and constructive comments were instrumental in improving the manuscript. Additionally, I am grateful to Equinor for supporting this work.

References

- Aanonsen, S. I., G. Nævdal, D. S. Oliver, A. C. Reynolds, and B. Vallès (2009). The ensemble Kalman filter in reservoir engineering—a review. *Spe Journal* 14(03), 393–412.
- Akaike, H. (1974). A new look at the statistical model identification. *IEEE transactions on automatic control* 19(6), 716–723.
- Amestoy, P. R., T. A. Davis, and I. S. Duff (2004). Algorithm 837: Amd, an approximate minimum degree ordering algorithm. *ACM Transactions on Mathematical Software (TOMS)* 30(3), 381–388.
- Anderson, J. L. (2003). A local least squares framework for ensemble filtering. *Monthly Weather Review* 131(4), 634–642.
- Baptista, R., Y. Marzouk, R. E. Morrison, and O. Zahm (2021). Learning non-Gaussian graphical models via Hessian scores and triangular transport. *arXiv preprint arXiv:2101.03093*.
- Baptista, R., Y. Marzouk, and O. Zahm (2020). On the representation and learning of monotone triangular transport maps. *arXiv preprint arXiv:2009.10303*.
- Burgers, G., P. J. Van Leeuwen, and G. Evensen (1998). Analysis scheme in the ensemble Kalman filter. *Monthly weather review* 126(6), 1719–1724.
- Claeskens, G. and N. L. Hjort (2008). Model selection and model averaging. *Cambridge Books*.
- Cuthill, E. and J. McKee (1969). Reducing the bandwidth of sparse symmetric matrices. In *Proceedings of the 1969 24th national conference*, pp. 157–172.
- Emerick, A. A. and A. C. Reynolds (2013). Ensemble smoother with multiple data assimilation. *Computers & Geosciences* 55, 3–15.

- Evensen, G. (1994). Sequential data assimilation with a nonlinear quasi-geostrophic model using Monte Carlo methods to forecast error statistics. *Journal of Geophysical Research: Oceans* 99(C5), 10143–10162.
- Evensen, G. (2003). The ensemble Kalman filter: Theoretical formulation and practical implementation. *Ocean dynamics* 53(4), 343–367.
- Evensen, G. et al. (2009). *Data assimilation: the ensemble Kalman filter*, Volume 2. Springer.
- Friedman, J. H. (2001). Greedy function approximation: a gradient boosting machine. *Annals of Statistics*, 1189–1232.
- Hamill, T. M., J. S. Whitaker, and C. Snyder (2001). Distance-dependent filtering of background error covariance estimates in an ensemble Kalman filter. *Monthly Weather Review* 129(11), 2776–2790.
- Hastie, T., J. Taylor, R. Tibshirani, and G. Walther (2007). Forward stagewise regression and the monotone lasso. *Electronic Journal of Statistics* 1, 1–29.
- Hastie, T., R. Tibshirani, and J. H. Friedman (2009). *The elements of statistical learning: data mining, inference, and prediction*, Volume 2. Springer.
- Hoerl, A. E. and R. W. Kennard (1970). Ridge regression: Biased estimation for nonorthogonal problems. *Technometrics* 12(1), 55–67.
- Houtekamer, P. L. and H. L. Mitchell (2001). A sequential ensemble Kalman filter for atmospheric data assimilation. *Monthly Weather Review* 129(1), 123–137.
- Houtekamer, P. L. and H. L. Mitchell (2005). Ensemble Kalman filtering. *Quarterly Journal of the Royal Meteorological Society* 131(613), 3269–3289.
- Huber, P. J. et al. (1967). The behavior of maximum likelihood estimates under nonstandard conditions. In *Proceedings of the fifth Berkeley symposium on mathematical statistics and probability*, Volume 1, pp. 221–233. Berkeley, CA: University of California Press.
- Hunt, B. R., E. J. Kostelich, and I. Szunyogh (2007). Efficient data assimilation for spatiotemporal chaos: A local ensemble transform Kalman filter. *Physica D: Nonlinear Phenomena* 230(1-2), 112–126.
- Kalman, R. (1960). A new approach to linear filtering and prediction problems. *Trans. ASME, D* 82, 35–44.
- Kalman, R. E. and R. S. Bucy (1961). New results in linear filtering and prediction theory. *Journal of Basic Engineering* 83(1), 95–108.
- Karypis, G. and V. Kumar (1998). A fast and high quality multilevel scheme for partitioning irregular graphs. *SIAM Journal on scientific Computing* 20(1), 359–392.
- Kleppe, T. S. (2024). Log-density gradient covariance and automatic metric tensors for Riemann manifold Monte Carlo methods. *Scandinavian Journal of Statistics*.
- Kloeden, P. E. and E. Platen (1992). *Numerical solution of stochastic differential equations*. Springer.
- Konishi, S. and G. Kitagawa (1996). Generalised information criteria in model selection. *Biometrika* 83(4), 875–890.
- Kristensen, K., A. Nielsen, C. W. Berg, H. Skaug, and B. M. Bell (2016). TMB: Automatic differentiation and Laplace approximation. *Journal of Statistical Software* 70(i05).
- Lindgren, F., D. Bolin, and H. Rue (2022). The SPDE approach for Gaussian and non-Gaussian fields: 10 years and still running. *Spatial Statistics*, 100599.
- Lindgren, F., H. Rue, and J. Lindström (2011). An explicit link between Gaussian fields and Gaussian Markov random fields: the stochastic partial differential equation approach. *Journal of the Royal Statistical Society: Series B (Statistical Methodology)* 73(4), 423–498.
- Lorenz, E. N. (1995). Predictability: A problem partly solved. In *Seminar on Predictability*, Shinfield Park, Reading. ECMWF.
- Lorenz, E. N. and K. A. Emanuel (1998). Optimal sites for supplementary weather observations: Simulation with a small model. *Journal of the Atmospheric Sciences* 55(3), 399–414.
- Lunde, B. Å. S., F. Curic, and S. Sortland (2022). GraphSPME: Markov precision matrix estimation and asymptotic Stein-type shrinkage. *arXiv preprint arXiv:2205.07584*.
- Marzouk, Y., T. Moselhy, M. Parno, and A. Spantini (2016). An introduction to sampling via measure transport. *arXiv preprint arXiv:1602.05023*.
- Mason, L., J. Baxter, P. Bartlett, and M. Frean (1999). Boosting algorithms as gradient descent. *Advances in neural information processing systems* 12.
- Moore, J. B. and B. Anderson (1979). *Optimal filtering*. Prentice-Hall New York.

- Øksendal, B. (2003). Stochastic differential equations. In *Stochastic differential equations*, pp. 65–84. Springer.
- Ott, E., B. R. Hunt, I. Szunyogh, A. V. Zimin, E. J. Kostelich, M. Corazza, E. Kalnay, D. Patil, and J. A. Yorke (2004). A local ensemble Kalman filter for atmospheric data assimilation. *Tellus A: Dynamic Meteorology and Oceanography* 56(5), 415–428.
- Raanes, P. N., A. S. Stordal, and R. J. Lorentzen (2023). Review of ensemble gradients for robust optimisation. *arXiv preprint arXiv:2304.12136*.
- Ramgraber, M., R. Baptista, D. McLaughlin, and Y. Marzouk (2023a). Ensemble transport smoothing. Part i: Unified framework. *Journal of Computational Physics: X* 17, 100134.
- Ramgraber, M., R. Baptista, D. McLaughlin, and Y. Marzouk (2023b). Ensemble transport smoothing. Part ii: Nonlinear updates. *Journal of Computational Physics: X* 17, 100133.
- Rosenblatt, M. (1952). Remarks on a multivariate transformation. *The Annals of Mathematical Statistics* 23(3), 470–472.
- Rozanov, J. A. (1977). Markov random fields and stochastic partial differential equations. *Mathematics of the USSR-Sbornik* 32(4), 515.
- Rue, H. and L. Held (2005). *Gaussian Markov random fields: theory and applications*. Chapman and Hall/CRC.
- Rue, H., S. Martino, and N. Chopin (2009). Approximate Bayesian inference for latent Gaussian models by using integrated nested Laplace approximations. *Journal of the Royal Statistical Society: Series B (Statistical Methodology)* 71(2), 319–392.
- Sebacher, B., R. Hanea, and A. S. Stordal (2017). An adaptive pluri-Gaussian simulation model for geological uncertainty quantification. *Journal of Petroleum Science and Engineering* 158, 494–508.
- Spantini, A., R. Baptista, and Y. Marzouk (2019). Coupling techniques for nonlinear ensemble filtering, arxiv. *arXiv preprint arXiv:1907.00389* 30.
- Spantini, A., D. Bigoni, and Y. Marzouk (2018). Inference via low-dimensional couplings. *The Journal of Machine Learning Research* 19(1), 2639–2709.
- Stone, M. (1974). Cross-validated choice and assessment of statistical predictions. *Journal of the Royal Statistical Society. Series B (Methodological)*, 111–147.
- Takeuchi, K. (1976). Distribution of information statistics and validity criteria of models. *Mathematical Science* 153, 12–18.
- Tibshirani, R. (1996). Regression shrinkage and selection via the lasso. *Journal of the Royal Statistical Society Series B: Statistical Methodology* 58(1), 267–288.
- Uhlenbeck, G. E. and L. S. Ornstein (1930). On the theory of the Brownian motion. *Physical Review* 36(5), 823.
- Van der Vaart, A. W. (2000). *Asymptotic statistics*, Volume 3. Cambridge University Press.